BIOMEMS (17BM831)

Hemanth Kumar G , Assistant Professor, Department of BME, ACSCE.

MODULE -4 : Materials for MEMS and Microsystems

Materials for MEMS and Microsystems: Substrates and wafers, Active Substrate materials, Silicon as a Substrate material – Ideal Substrate, Crystal Structure, Mechanical Properties of Silicon, Silicon Compounds, Silicon Peizoresistors, Gallium Arsenide, Quartz, Polymers, Packaging Materials.

This chapter will cover the materials used in "silicon-based" MEMS and microsystems. As such, silicon will be the principal material to be studied.

Other materials to be dealt with are silicon compounds such as: SiO_2, SiC, Si_3N_4 and polysilicon.

Also will be covered are electrically conducting of silicon piezoresistors and piezoelectric crystals for electromechanical actuations and signal transductions.

An overview of polymers, which are the "rising stars" to be used as MEMS and microsystems substrate materials, will be studied too.

Silicon – an ideal substrate material for MEMS

- Silicon (Si) is the most abundant material on earth. It almost always exists in compounds with other elements.

- Single crystal silicon is the most widely used substrate material for MEMS and microsystems.

- The popularity of silicon for such application is primarily for the following reasons:

  (1) It is mechanically stable and it is feasible to be integrated into electronics on the same substrate (b/c it is a semiconducting material).

  (2) Electronics for signal transduction such as the p or n-type piezoresistive can be readily integrated with the Si substrate-ideal for transistors.

  (3) Silicon is almost an ideal structure material. It has about the same Young's modulus as steel ($\sim 2 \times 10^5$ MPa), but is as light as aluminum with a density of about 2.3 g/cm^3.

Silicon – an ideal substrate material for MEMS-Cont'd

(4) It has a melting point at 1400°C, which is about twice higher than that of aluminum. This high melting point makes silicon dimensionally stable even at elevated temperature.

(5) Its thermal expansion coefficient is about 8 times smaller than that of steel, and is more than 10 times smaller than that of aluminum.

(6) Silicon shows virtually no mechanical hysteresis. It is thus an ideal candidate material for sensors and actuators.

(7) Silicon wafers are extremely flat for coatings and additional thin film layers for either being integral structural parts, or performing precise electromechanical functions.

(8) There is a greater flexibility in design and manufacture with silicon than with other substrate materials. Treatments and fabrication processes for silicon substrates are well established and documented.

Single-Crystal Silicon

- For silicon to be used as a substrate material in integrated circuits and MEMS, it has to be in a pure single-crystal form.
- The most commonly used method of producing single-crystal silicon is the Czochralski (CZ) method.

The Czochralski method for producing single-crystal silicon

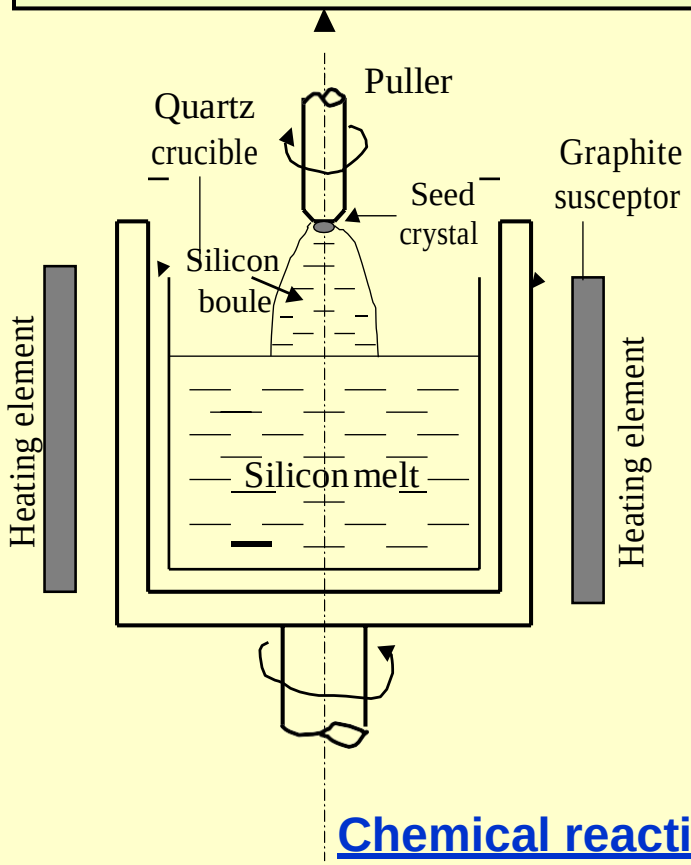

Equipment: a crucible and a "puller".

Procedure:

(1) Raw Si (quartzite) + coal, coke, woodchips) are melted in the crucible.

(2) A "seed" crystal is brought to be in contact with molten Si to form larger crystal.

(3) The "puller" slowly pulls the molten Si up to form pure Si "boule" after the solidification.

(4) The diameters of the "bologna-like" boules vary from 100 mm (4") to 300 mm (12") in diameters.

Chemical reaction for the process: $SiC + SiO_2 \rightarrow Si + CO + SiO$

Pure silicon wafers

Pure silicon boules of 300 mm diameter and 30 ft long, can weigh up to 400 Kg.

These boules are sliced into thin disks (wafers) using diamond saws.

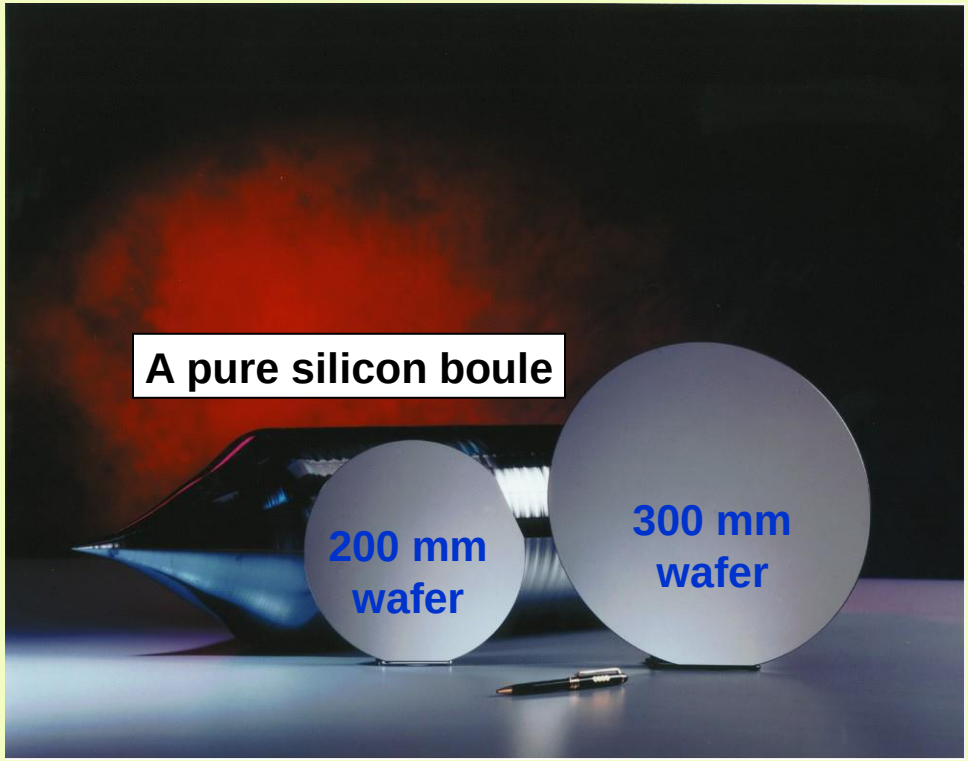

Standard sizes of wafers are:

100 mm (4”) diameter x 500 μm thick.
150 mm (6”) diameter x 750 μm thick.
200 mm (8”) diameter x 1 mm thick
300 mm (12”) diameter x 750 μm thick (tentative).

Single Silicon Crystal Structure

- **Single silicon crystals are basically of "face-cubic-center" (FCC) structure.**
- **The crystal structure of a typical FCC crystal is shown below:**

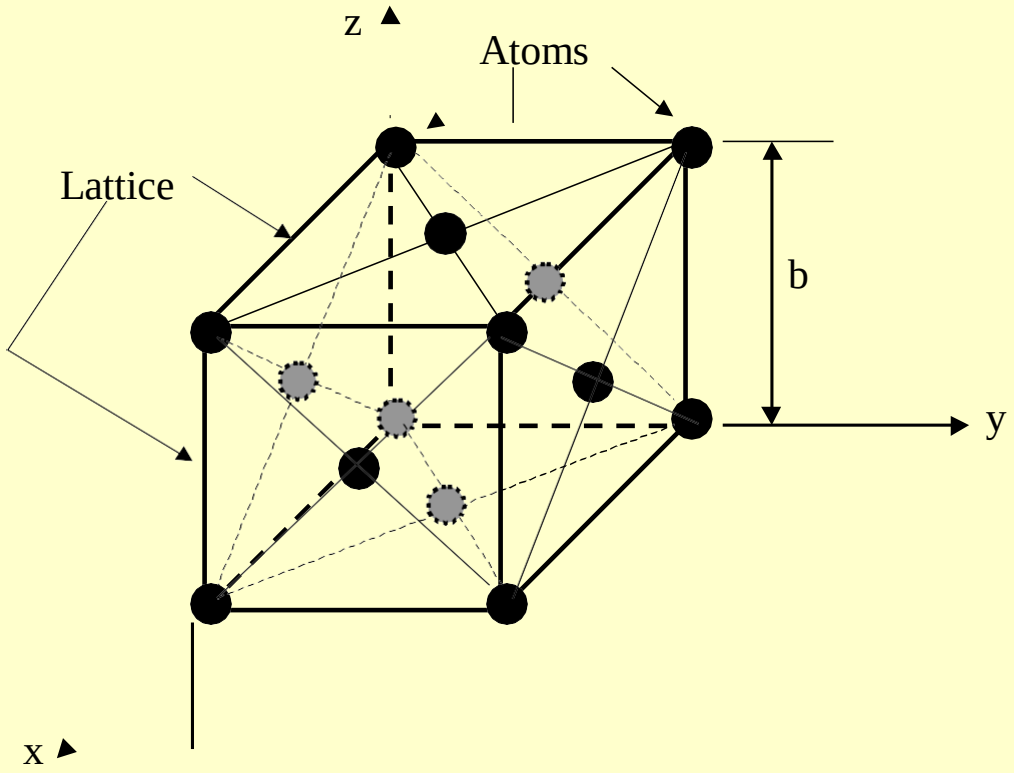

Note: Total number of atoms: 8 at corners and 6 at faces = **14 atoms**

Single Silicon Crystal Structure-Cont'd

- Single crystal silicon, however has 4 extra atoms in the interior.
- The situation is like to merge two FCC crystals together as shown below:

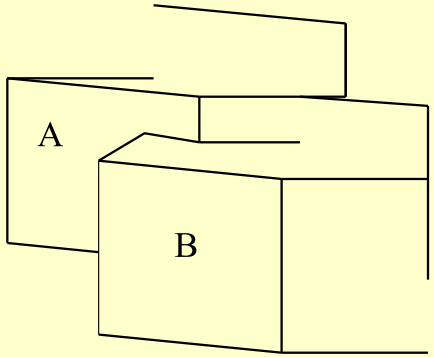

(a) Merger of two FCC

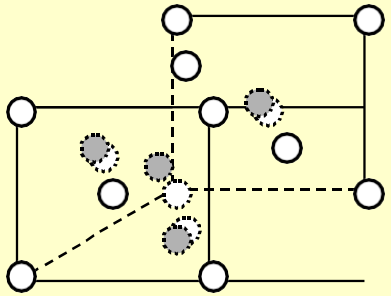

(b) Merged crystal structure

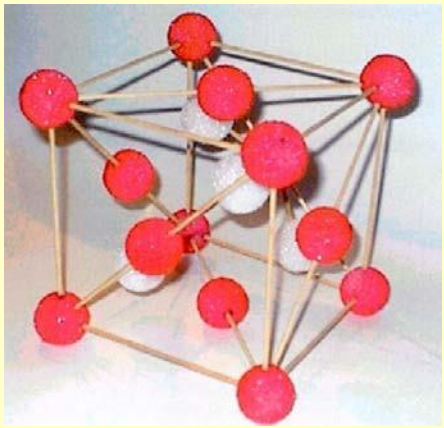

- Total no. of atoms in a single silicon crystal = 18.
- The unsymmetrical distribution of atoms within the crystal make pure silicon anisotropic in its mechanical properties.
- In general, however, we treat silicon as an isotropic material.

The Miller Indices

- Miller indices are commonly use to describe the **faces** of crystalline materials.

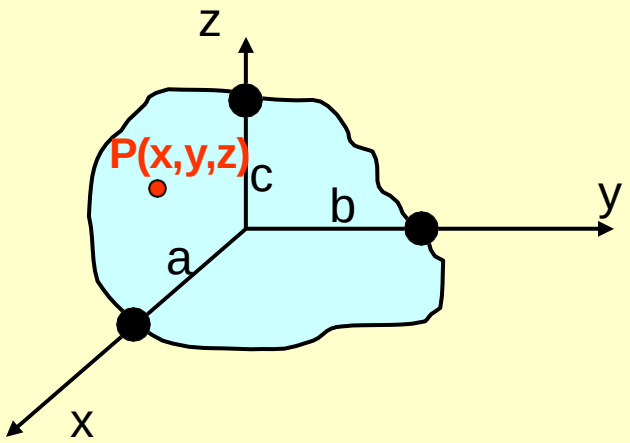

- A plane intersects x, y and z-coordinates at a, b and c.
- A point on the plane located at P(x,y,z)
- The equation defines the P(x,y,z) is:

$$\frac{x}{a}+\frac{y}{b}+\frac{z}{c}=1 \qquad (7.1)$$

Express Eq. (7.1) in a different form:

$$hx + ky + mz = 1 \qquad (7.2)$$

in which h = 1/a, k = 1/b and k = 1/c.

- Miller indices involve:

  (hkm) = designation of a “face”, or a **plane**;

  <hkm> = designation of a **direction** that is perpendicular to the (hkm) plane.

- **NOTE:** In a cubic crystal, such as silicon, a = b = c = 1

The 3 Distinct Planes of a Cubic Crystal

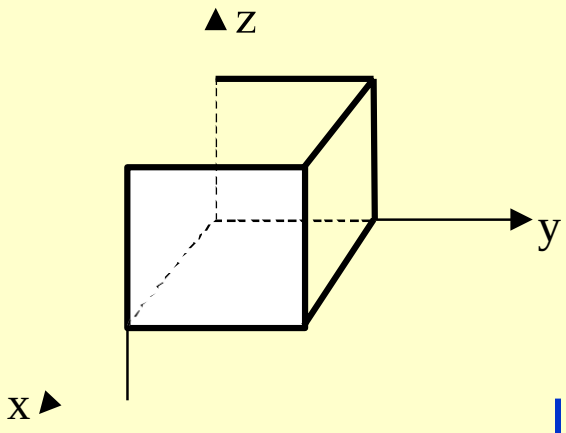

Figure A

Top face: Plane (001)

Right face: Plane (010)

Front face: **Plane (100)**

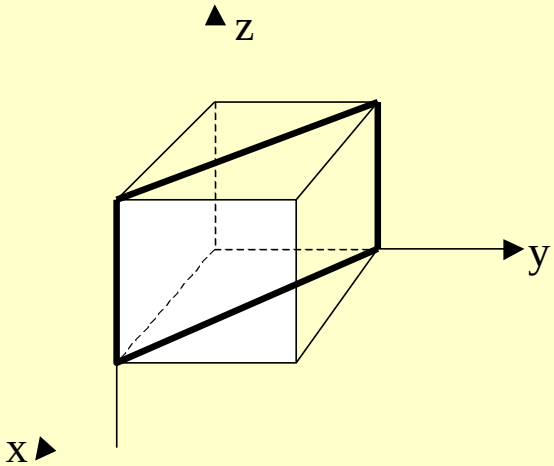

Figure B

Diagonal face: **Plane (110)**

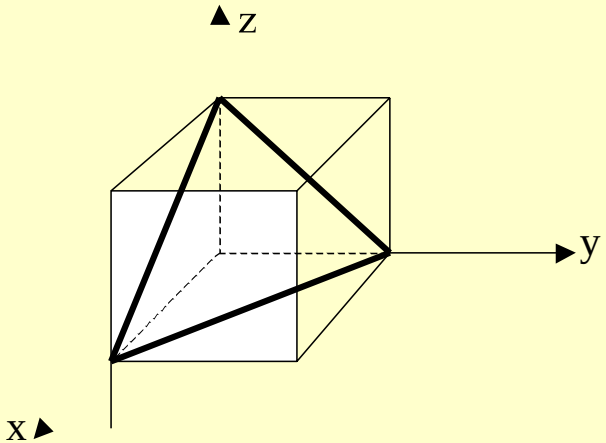

Figure C

Incline face:
Plane (111)

The 3 Principal Planes of a Silicon Crystal

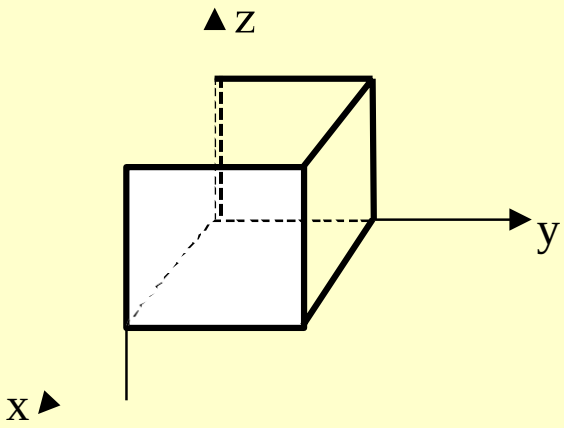

The (100) group

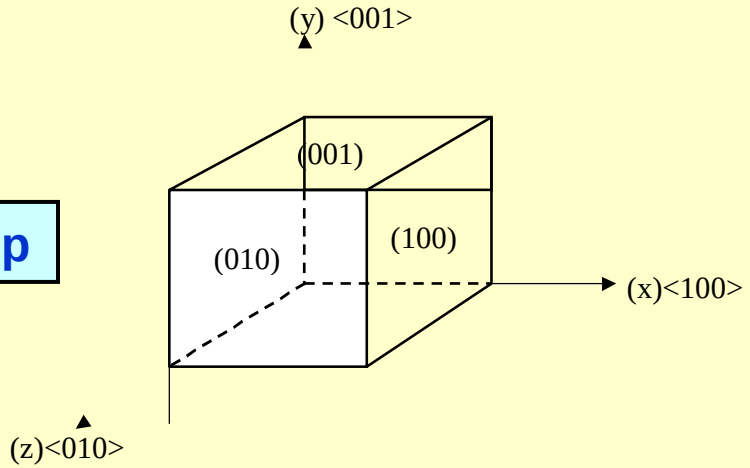

The (110) group

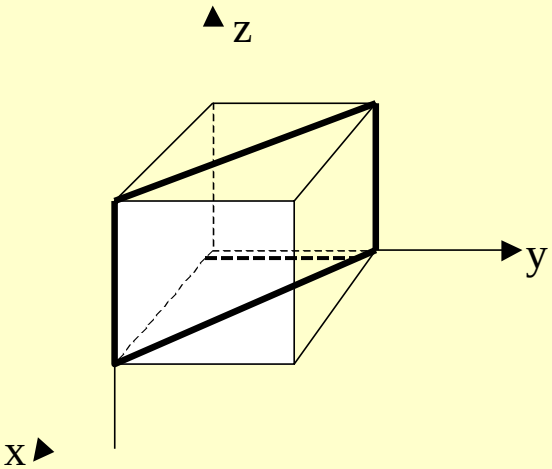

The (111) group

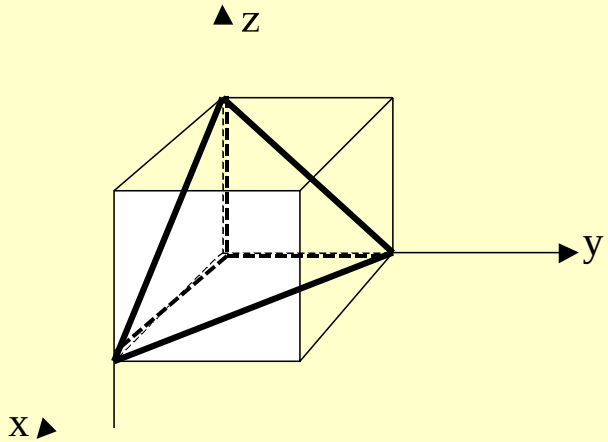

The 3 Principal Planes of a Silicon Crystal-Cont'd

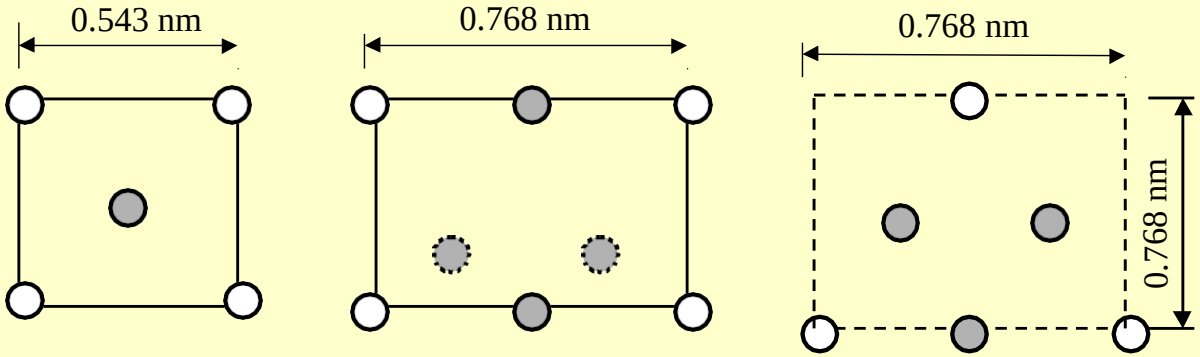

(100) Plane

(110) Plane
Diagonal Plane

(111) Plane
Inclined Plane

- **Characteristics of silicon by principal planes:**

(1) The **(100)** planes contain least number of atoms→ the weakest plane → **easiest to work with**.

(2) The **(110)** planes offers the **cleanest surfaces** in micro fabrications.

(3) The **(111)** contains shortest bonds between atoms → **strongest plane** → toughest to work with.

Miller Index for Orientation	Young's Modulus, E (GPa)	Shear Modulus, G (GPa)
<100>	**129.5**	79.0
<110>	168.0	61.7
<111>	**186.5**	57.5

NOTE: The (100) plane makes an angle of 54.74° with the (111) plane.

(Bulk) Mechanical and Thermophysical Properties of Silicon

Legend: σ_y = yield strength; E = Young's modulus; ρ = mass density; C = specific heat; k = thermal conductivity; α = coefficient of thermal expansion, T_M = melting point.

	σ_y (10^9 N/m^2)	E (10^{11} N/m^2)	ρ (g/cm^3)	C (J/g-^{o}C)	k (W/cm-^{o}C)	α (10^{-6}/^{o}C)	T_M (^{o}C)
Si	7.00	1.90	2.30	0.70	1.57	2.33	1400
SiC	21.00	7.00	3.20	0.67	3.50	3.30	2300
Si_3N_4	14.00	3.85	3.10	0.69	0.19	0.80	1930
SiO_2	8.40	0.73	2.27	1.00	0.014	0.50	1700
Aluminum	0.17	0.70	2.70	0.942	2.36	25	660
Stainless Steel	2.10	2.00	7.90	0.47	0.329	17.30	1500
Copper	0.07	0.11	8.9	0.386	3.93	16.56	1080
GaAs	2.70	0.75	5.30	0.35	0.50	6.86	1238
Ge		1.03	5.32	0.31	0.60	5.80	937
Quartz	0.5-0.7	0.76-0.97	2.66	0.82-1.20	0.067-0.12	7.10	1710

* Principal source for semiconductor material properties: "Fundamentals of Microfabrication", Marc Madou, CRC Press, 1997

Silicon Compounds

There are **3** principal silicon compounds used in MEMS and microsystems: Silicon dioxide (**SiO_2**), Silicon carbide (**SiC**) and silicon nitride (**Si_3N_4**) – each Has distinct characteristic and unique applications.

Silicon dioxide (SiO_2)

- **It is least expensive material to offer good thermal and electrical insulation.**
- **Also used a low-cost material for "masks" in micro fabrication processes such as etching, deposition and diffusion.**
- **Used as sacrificial material in "surface micromachining".**
- **Above all, it is very easy to produce:**

- by dry heating of silicon: $Si + O_2 \rightarrow SiO_2$

- or by oxide silicon in wet steam: $Si + 2H_2O \rightarrow SiO_2 + 2H_2$

Silicon dioxide (SiO_2) – cont'd

Properties	Values
Density (g/cm^3)	2.27
Resistivity (Ω-cm)	$\geq 10^{16}$
Dielectric constant	3.9
Melting point (^oC)	~1700
Specific heat ($J/g/^oC$)	1.0
Thermal conductivity ($W/cm/^oC$)	0.014
Coefficient of thermal expansion ($ppm/^oC$)	0.5

Silicon carbide (SiC)

Its very **high melting point** and resistance to chemical reactions make it ideal candidate material for being masks in micro fabrication processes.

It has **superior dimensional stability**.

Silicon nitride (Si_3N_4)

- **Produced by chemical reaction:**

$$3SiCl_2H_2 + 4NH_3 \longrightarrow Si_3N_4 + 6HCL + 6H_2$$

- **Used as excellent barrier to diffusion to water and ions.**
- **Its ultra strong resistance to oxidation and many etchants make it a superior material for masks in deep etching.**
- **Also used as high strength electric insulators.**
- **Selected properties Si_3N_4 films are as follows:**

Properties	LPCVD*	PECVD**
Deposition temperature (°C)	700-800	250-350
Density (g/cm^3)	2.9-3.2	2.4-2.8
Film quality	Excellent	Poor
Dielectric constant	6-7	6-9
Resistivity (Ω-cm)	10^{16}	10^6-10^{15}
Refractive index	2.01	1.8-2.5
Atom % H	4-8	20-25
Etch rate in concentrated HF	200 A/min	
Etch rate in boillng HF	5-10A/min	
Poisson's ratio	0.27	
Young's modulus (GPa)	385	
Coefficient of thermal expansion, ppm/°C	1.6	

* Low pressure chemical vapor deposition; ** Plasma enhanced chemical vapor deposition

Polycrystalline silicon

- It is usually called "Polysilicon".
- It is an aggregation of pure silicon crystals with randomly orientations deposited on the top of silicon substrates:

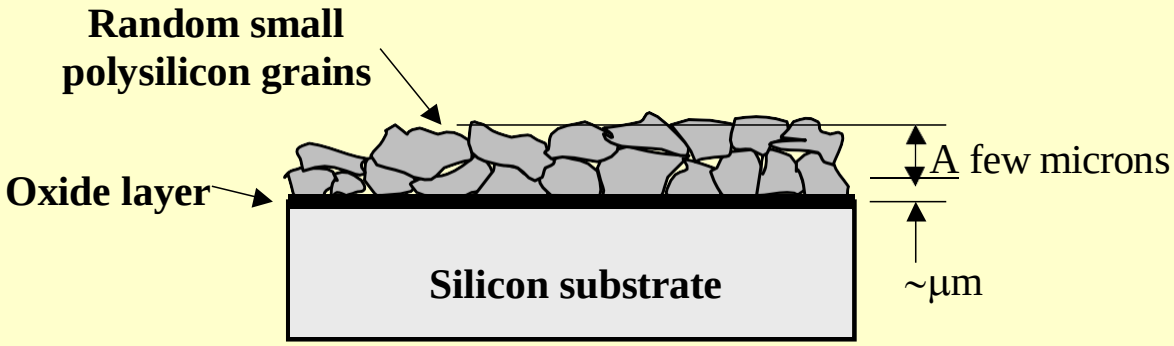

- These polysilicon usually are highly doped silicon.
- They are deposited to the substrate surfaces to produce localized "resistors" and "gates for transistors"
- Being randomly oriented, polysilicon is even stronger than single silicon crystals.

Polycrystalline silicon – cont'd

Comparison of Mechanical Properties of Polysilicon with Other Materials

Materials	Young's modulus (GPa)	Poisson's ratio	Coefficient of thermal expansion (ppm/°C)
As substrates:			
Silicon	190	0.23	2.6
Alumina	415		8.7
Silica	73	0.17	0.4
As thin films:			
Polysilicon	***160***	***0.23***	***2.8***
Thermal SiO_2	70	0.2	0.35
LPCVD SiO_2	270	0.27	1.6
PACVD SiO_2			2.3
Aluminum	70	0.35	25
Tungsten	410	0.28	4.3
Polymide	3.2	0.42	20-70

Silicon Piezoresistors

Piezoresistance = **a change in electrical resistance of solids when subjected to stress fields. Doped silicon are piezoresistors (p-type or n-type).**

Relationship between change of resistance {ΔR} and stresses {σ}:

$$\{\Delta R\} = [\pi]\{\sigma\} \qquad (7\text{-}6)$$

where $\{\Delta R\} = \{\Delta R_{xx} \;\; \Delta R_{yy} \;\; \Delta R_{zz} \;\; \Delta R_{xy} \;\; \Delta R_{xz} \;\; \Delta R_{yz}\}^T$ represents the change of resistances in an infinitesimally small cubic piezoresistive crystal element with corresponding stress components:
$\{\sigma\} = \{\sigma_{xx} \;\; \sigma_{yy} \;\; \sigma_{zz} \;\; \sigma_{xy} \;\; \sigma_{xz} \;\; \sigma_{yz}\}^T$ and **[π] = piezoresistive coefficient matrix**.

A silicon piezoresistance subjected to a stress field:

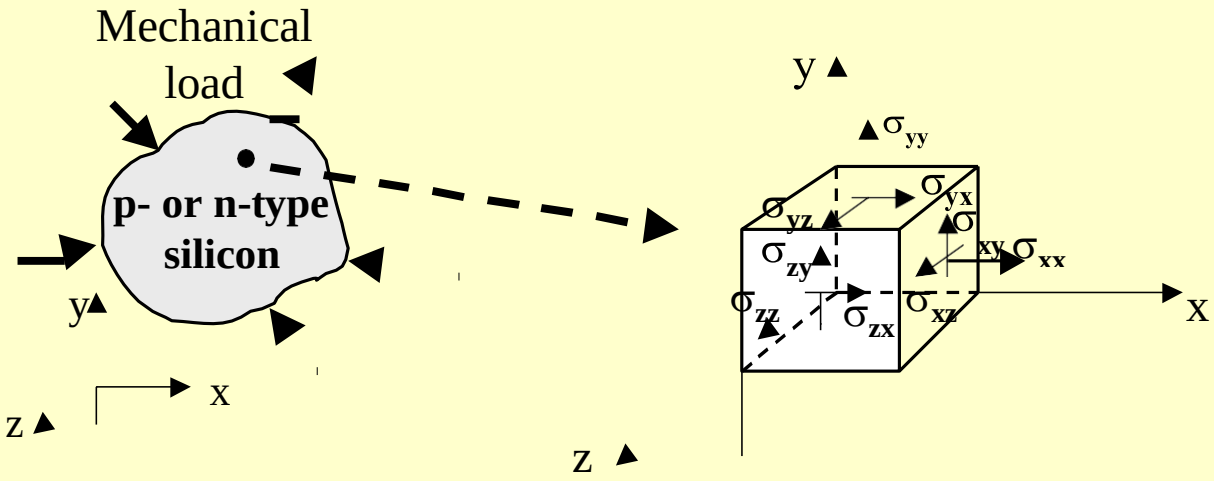

Silicon Piezoresistors – Cont'd

- Due to equilibrium condition, there are six independent stress components: 3 normal stress components and 3 shearing stress components.
- Consequently, the **piezoresistive coefficient matrix** has the components:

$$[\pi] = \begin{bmatrix} \pi_{11} & \pi_{12} & \pi_{12} & 0 & 0 & 0 \\ \pi_{12} & \pi_{11} & \pi_{12} & 0 & 0 & 0 \\ \pi_{12} & \pi_{12} & \pi_{11} & 0 & 0 & 0 \\ 0 & 0 & 0 & \pi_{44} & 0 & 0 \\ 0 & 0 & 0 & 0 & \pi_{44} & 0 \\ 0 & 0 & 0 & 0 & 0 & \pi_{44} \end{bmatrix} \qquad (7.7)$$

- Expanding Eq. (7.6) result in the following:

$$\Delta R_{xx} = \pi_{11}\sigma_{xx} + \pi_{12}\left(\sigma_{yy} + \sigma_{zz}\right) \qquad \Delta R_{xy} = \pi_{44}\,\sigma_{xy}$$

$$\Delta R_{yy} = \pi_{11}\sigma_{yy} + \pi_{12}\left(\sigma_{xx} + \sigma_{zz}\right) \qquad \Delta R_{xz} = \pi_{44}\,\sigma_{xz}$$

$$\Delta R_{zz} = \pi_{11}\sigma_{11} + \pi_{12}\left(\sigma_{xx} + \sigma_{yy}\right) \qquad \Delta R_{yz} = \pi_{44}\,\sigma_{yz}$$

- Note: Only **3** piezoresistive coefficients are required; π_{11} and π_{12} associated with normal stresses and π_{44} with shearing stresses.

Silicon Piezoresistors – Cont'd

Numerical values of piezoresistive coefficients

Silicon piezoresistors at room temperature

Materials	Resistivity (Ω-cm)	π_{11}*	π_{12}*	π_{44}*
p-silicon	7.8	+6.6	-1.1	+138.1
n-silicon	11.7	-102.2	+53.4	-13.6

Silicon piezoresistors

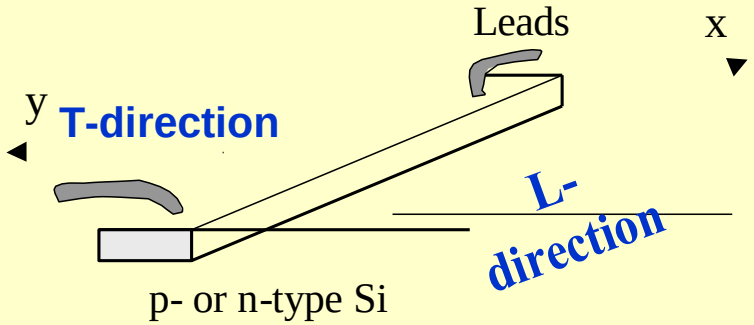

$$\frac{\Delta R}{R} = \pi_L \sigma_L + \pi_T \sigma_T$$

Silicon Piezoresistors – Cont'd

Numerical values of piezoresistive coefficients

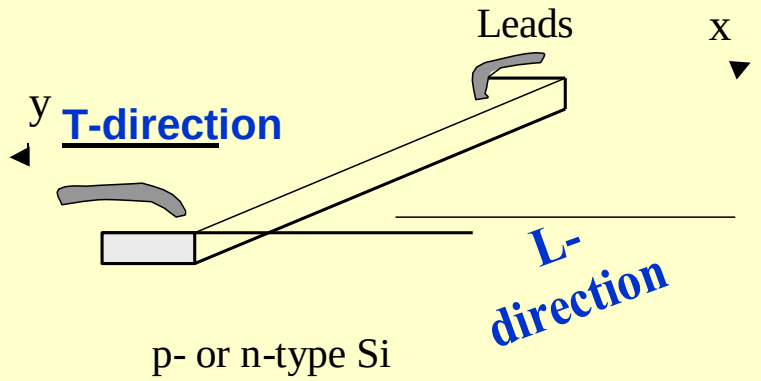

$$\frac{\Delta R}{R} = \pi_L \sigma_L + \pi_T \sigma_T$$

Piezoresistive coefficients of p-type silicon piezorestors in various directions

Crystal Planes	Orientation <x>	Orientation <y>	π_L	π_T
(100)	<111>	<111>	$+0.66\pi_{44}$	$-0.33\pi_{44}$
(100)	<110>	<100>	$+0.5\pi_{44}$	~0
(100)	<110>	<110>	$+0.5\pi_{44}$	$-0.5\pi_{44}$
(100)	<100>	<100>	$+0.02\pi_{44}$	$+0.02\pi_{44}$

Example 7.3 **Estimate the change of resistance in silicon piezoresistors attached to the diaphragm of a pressure sensor in Example 4.4.**

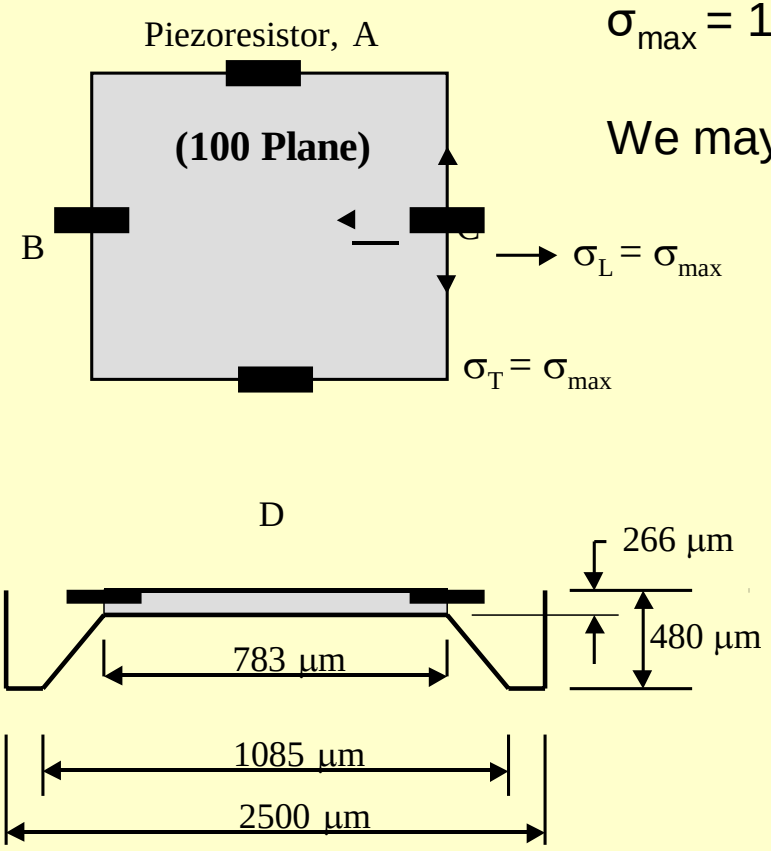

From Example 4.4, the corresponding maximum stress at the mid-span of each of the 4 edges is:
σ_{max} = 186.81 MPa with an applied pressure at 70 MPa.

We may thus let: $\boldsymbol{\sigma_L = \sigma_T = \sigma_{max}}$ = 186.8 MPa, or

$\boldsymbol{= 186.8 \times 10^6}$ **Pa** (N/m^2)

Since the diaphragm is on (100) face, the two piezoresistive coefficients are:

$$\pi_L = \pi_T = 0.02\ \pi_{44}$$

But $\pi_{44} = 138.1 \times 10^{-11}$ Pa^{-1} from the Table, we thus have:

$$\frac{\Delta R}{R} = \pi_L \sigma_L + \pi_T \sigma_T = 2\pi_{44}\sigma_{max} = 2 \times 0.02(138.1 \times 10^{-11})(186.8 \times 10^6) = 0.01032 \quad \Omega/\Omega$$

Temperature sensitivity of silicon piezoresistors

A major deficiency of silicon piezoresistors is its sensitivity of temperature as indicated in the table:

Doping concentration ($10^{18}/cm^3$)	p-Type TCR (% per ^oC)	p-Type TCP (% per ^oC)	n-Type TCR (% per ^oC)	n-Type TCP (% per ^oC)
5	0.0	-0.27	0.01	-0.28
10	0.01	**-0.27**	0.05	-0.27
30	0.06	-0.18	0.09	-0.18
100	0.17	-0.16	0.19	-0.12

TCR = temperature coefficient of resistance;
TCP = temperature coefficient of piezoresistivity.

Example: a p-type silicon piezoresistor with a doping of 10^{19} atoms/cm^3,
The loss of piezoresistivity is **0.27%/^{o}C**. In an operating temperature of 120^{o}C,
It would lose (120-20)x0.27% = 27% of the value of the piezoresistivity coefficient.

Gallium Arsenide (GaAs)

- **GaAs is a compound simiconductor with equal number of Ga and As atoms.**
- **Because it is a compound, it is more difficult to process.**
- **It is excellent material for monolithic integration of electronic and photonic devices on a single substrate.**
- **The reason for being excellent material for photoelectronics is its high electron mobility (7 times more mobile than silicon):**

Materials	Electron Mobility, m^2/V-sec
Aluminum	0.00435
Copper	0.00136
Silicon	0.145
Gallium Arsenide, GaAs	***0.850***
Silicon oxide	≅ 0
Silicon nitride	≅ 0

Gallium Arsenide (GaAs)-Cont'd

- **GaAs is also a good thermal insulator.**
- **Low yield strength (only 1/3 of that of silicon) – "bad".**
- **A comparison of GaAs and silicon as substrate materials in micromachining:**

Properties	GaAs	Silicon
Opto-electronics	Very good	Not good
Piezoelectric effect	Yes	No
Piezoelectric coefficient (pN/^{o}C)	2.6	Nil
Thermal conductivity	Relatively low	Relatively high
Cost	High	Low
Bonding to other substrates	Difficult	Relatively easy
Fracture	Brittle, fragile	Brittle, strong
Operating temperature	High	Low
Optimum operating temp. (^{o}C)	460	300
Physical stability	Fair	Very good
Hardness (GPa)	7	10
Fracture strength (GPa)	2.7	6

Quartz

- **Quartz is a compound of SiO_2.**
- **The single-unit cell is in shape of tetrahedron:**
- **Quartz crystal is made of up to 6 rings with**

  6 silicon atoms.

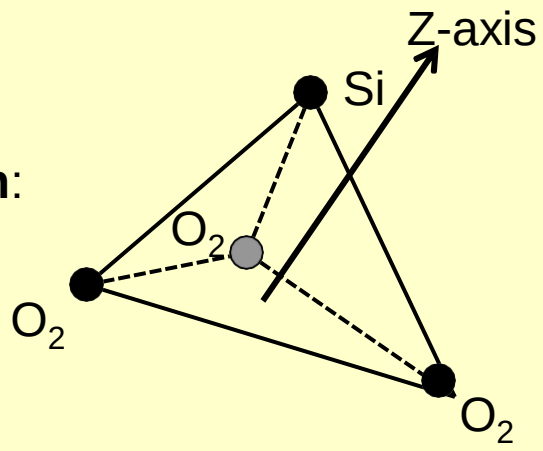

Properties	Value ∥ Z	Value ⊥ Z	Temperature Dependency
Thermal conductivity (Cal/cm/sec/^{o}C)	$29x10^{-3}$	$16x10^{-3}$	↓with T
Relative permittivity	4.6	4.5	↓with T
Density (Kg/m^3)	$2.66x10^3$	$2.66x10^3$	
Coefficient of thermal expansion (ppm/^{o}C)	7.1	13.2	↑with T
Electrical resistivity (Ω/cm)	$0.1x10^{15}$	$20x10^{15}$	↓with T
Fracture strength (GPa)	1.7	1.7	↓with T
Hardness (GPa)	12	12	

Quartz-Cont'd

- Quartz is ideal material for sensors because of its extreme dimensional stability.
- It is used as piezoelectric material in many devices.
- It is also excellent material for microfluics systems used in biomedical applications.
- It offers excellent electric insulation in microsystems.
- A major disadvantage is its hard in machining. It is usually etched in HF/NH4F into desired shapes.
- Quartz wafers up to 75 mm diameter by 100 μm thick are available commercially.

Piezoelectric Crystals

- Piezoelectric crystals are solid ceramic compounds that produce piezoelectric effects:

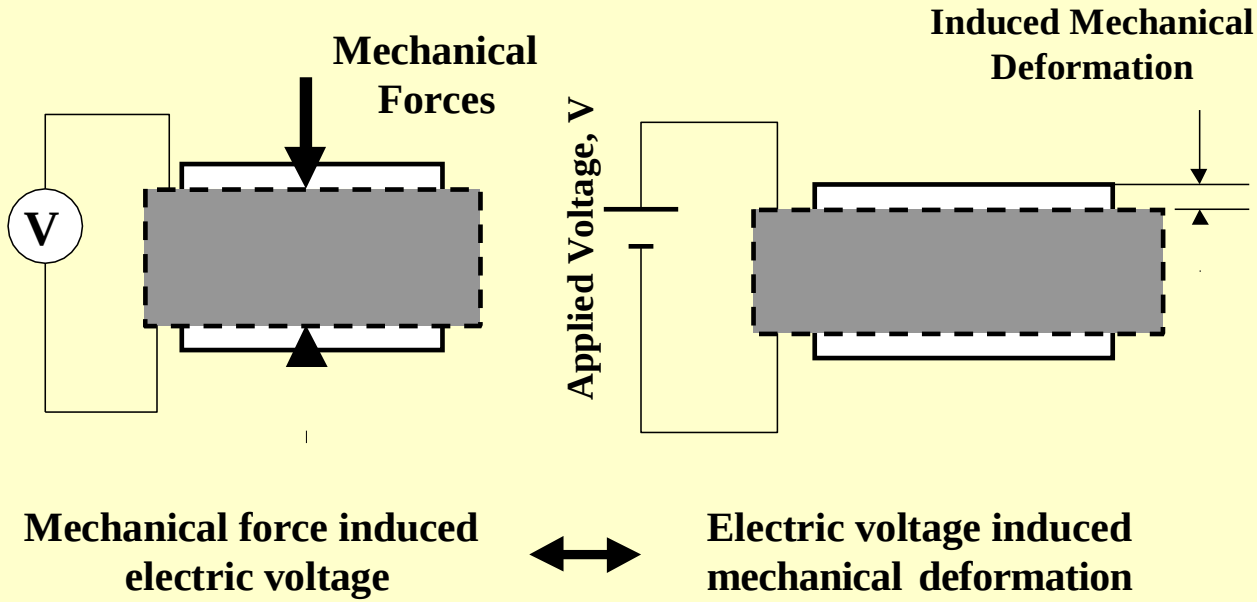

- Natural piezoelectric crystals are: quartz, tourmaline and sodium potassium tartrate.

- Synthesized crystals are: Rochelle salt, barium titanate and lead zirconate.

Piezoelectric Crystals – Cont'd

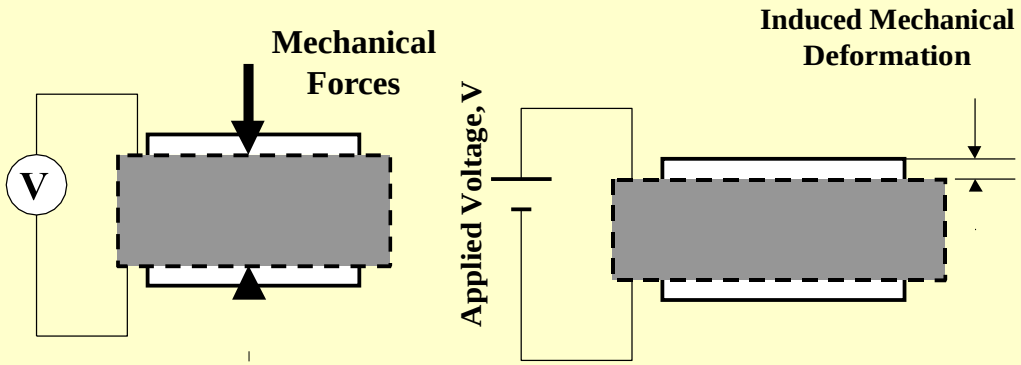

Mechanical strain by electric field:

$$\varepsilon = d\,V$$

where ε = induced strain
d = piezoelectric coefficient
V = applied voltage, V/m

Electric field by stress:

$$V = f\,\sigma$$

where V = generated voltage in volts/m
σ = applied stress in Pa

$$\frac{1}{fd} = E$$

Piezoelectric Crystals – Cont'd

Piezoelectric coefficients:

Piezoelectric Crystals	Coefficient, d (10^{-12} m/volt)	Electromechanical conversion factor, K**
Quartz (crystal SiO_2)	2.3	0.1
Barium titnate ($BaTiO_3$)	100-190	0.49
Lead zirconate titanate, PZT ($PbTi_{1-x}Zr_xO_3$)	480	0.72
$PbZrTiO_6$	250	
$PbNb_2O_6$	80	
Rochelle salt ($NaKC_4H_4O_6$-$4H_2O$)	350	0.78
Polyvinylidene fluorid, PVDF	18	

** $K^2 = \frac{Output\ of\ mechanical\ energy}{Input\ of\ electrical\ energy}$ or $K^2 = \frac{Output\ of\ electrical\ energy}{Input\ of\ mechanical\ energy}$

Example 7.4

A thin piezoelectric crystal film, **PZT** is used to transduce the signal in a micro accelerometer involving a cantilever beam made of silicon. The accelerometer is design for maximum acceleration/deceleration of **10 g**.

The PZT transducer is located at the support of the cantilever beam where the maximum strain exists (near the support) during the bending of the beam as illustrated below.

Determine the electrical voltage output from the PZT film at a maximum acceleration/deceleration of 10 g.

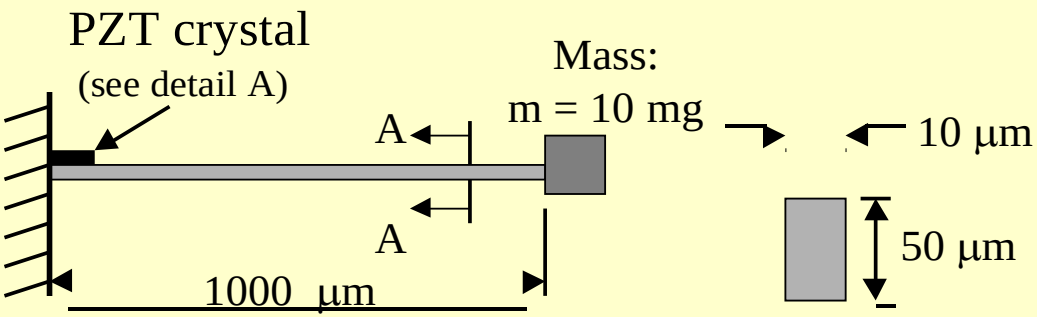

View A-A

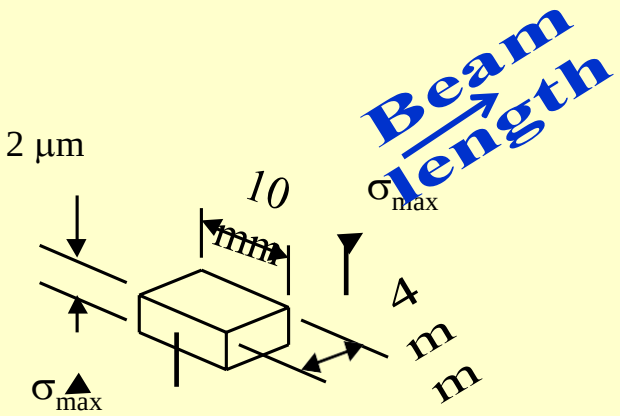

Detail A

Example 7.4 – Cont'd

Solution:

Use Newton's 2nd law to find the **equivalent dynamic force** with an acceleration of 10 g: $P_{eq} = ma = (10x10^{-6})x(10x9.81) = 981x10^{-6}$ N

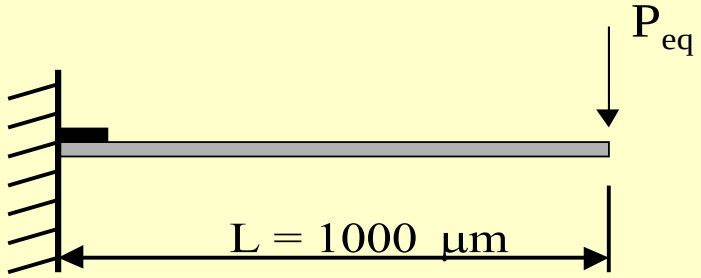

The **maximum bending moment** is:

$M_{max} = P_{eq}L = (981x10^{-6})(1000x10^{-6}) = 0.981x10^{-6}$ N-m and it occurs at the built-in end

The corresponding **maximum stress** is:

$$\sigma_{\max} = \frac{M_{\max} C}{I} = \frac{(0.981x10^{-6})(25x10^{-6})}{(0.1042x10^{-18})} = 235.36x10^{6} \text{ Pa}$$

and the **maximum strain** is: $\varepsilon_{\max} = \frac{\sigma_{\max}}{E} = \frac{235.36x10^{6}}{1.9x10^{11}} = 123.87x10^{-5}$ m/m

The **voltage** generated in the PZT piezoelectric crystal is:

$$V = \frac{\varepsilon}{d} = \frac{\varepsilon_{\max}}{d} = \frac{123.87x10^{-5}}{480x10^{-12}} = 0.258x10^{7} \text{ Volts/m}$$

or $v = VI = (0.258x10^{7})(4x10^{-6}) = 10.32$ volts

Example 7.5

Determine the **required electric voltage** for ejecting a droplet of ink from an inkjet printer head using **PZT** piezoelectric crystal as a pumping mechanism.

The ejected ink will have a resolution of **300 dpi** (dots per inch). The ink droplet is assumed to produce **a dot with a film thickness of 1 μm** on the paper.

The geometry and dimension of the printer head is illustrated below. Assume that the **ink droplet takes a shape of a sphere** and the inkwell is always re-filled after ejection.

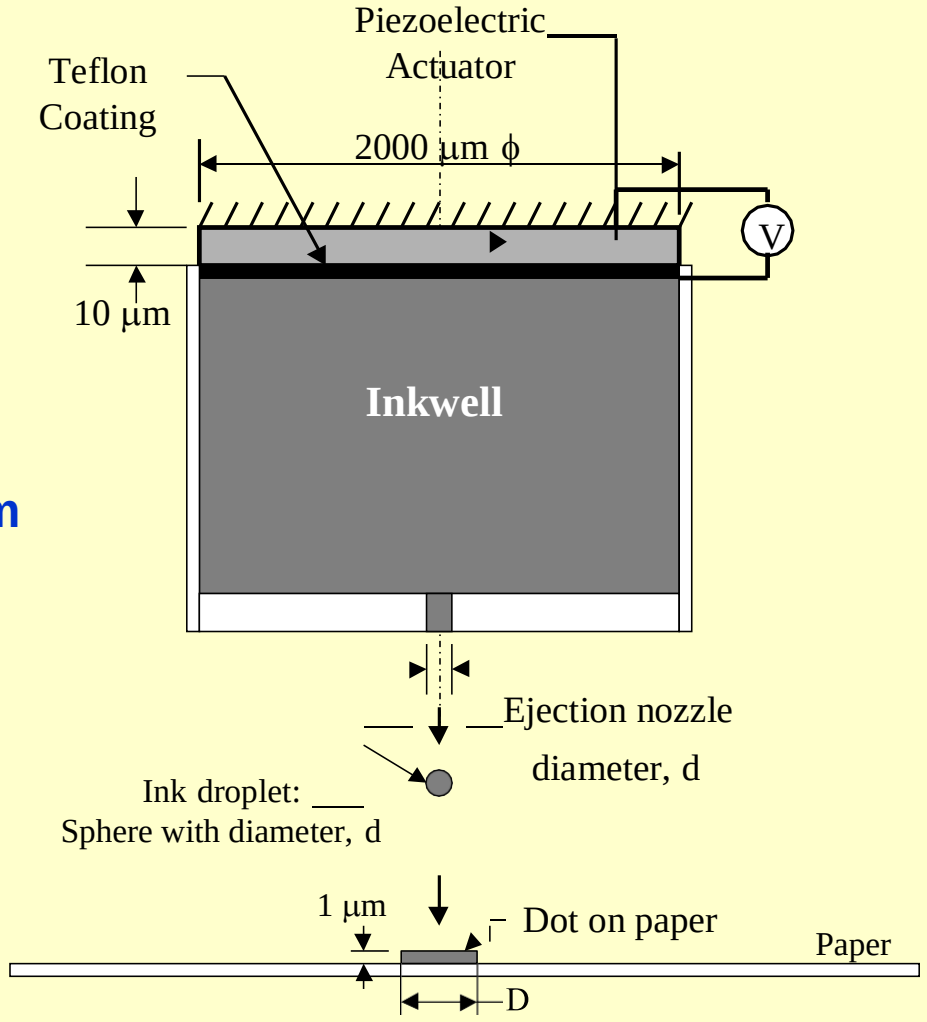

Example 7.5 – Cont'd

Solution:

- **Determine the ejection nozzle diameter, d:**

The diameter of the dot film on the paper is:

D = 1/300 inch = 0.084666 mm = 84.67 μm

By **equating the volumes** of the dot sphere the flat dot on the paper, we have:

$$\frac{4}{3}\pi r^3 = \frac{\pi}{4} D^2 (t)$$

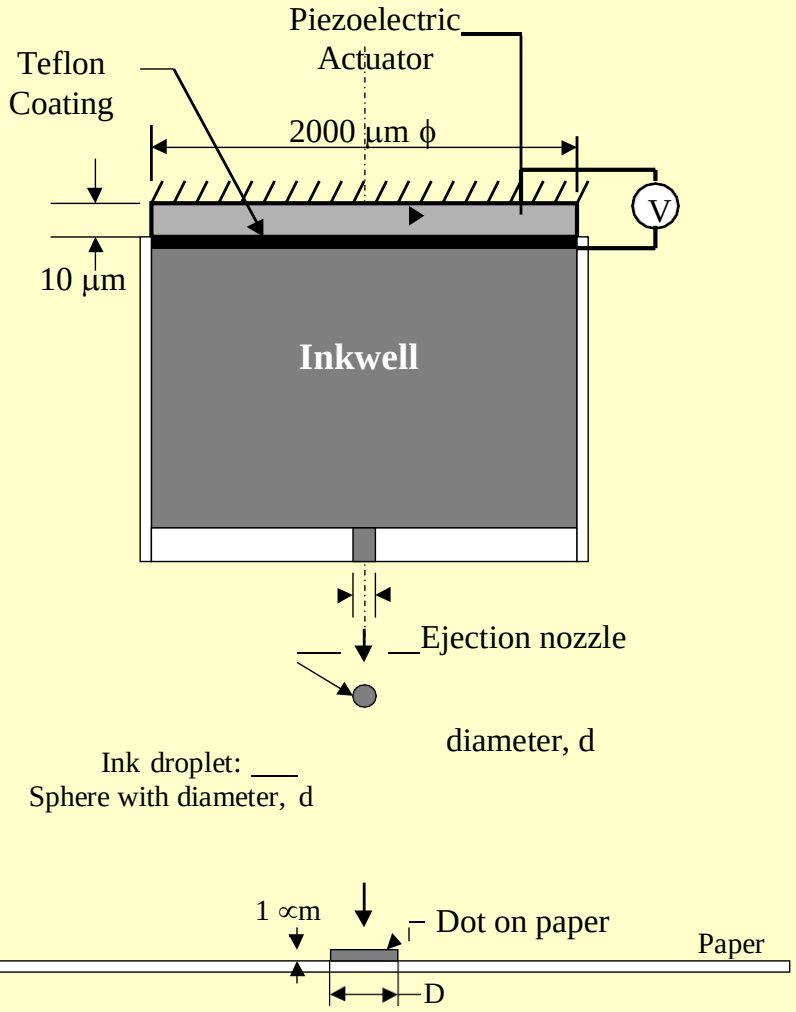

from which, we get the radius of the dot, r = 11.04x10^{-6} m, with D = 84.7 μm and t = 1 μm

Example 7.5 – Cont'd

- We assume that:

Volume of an ink droplet leaving the ink well

= **Volume created by vertical expansion of the PZT cover**

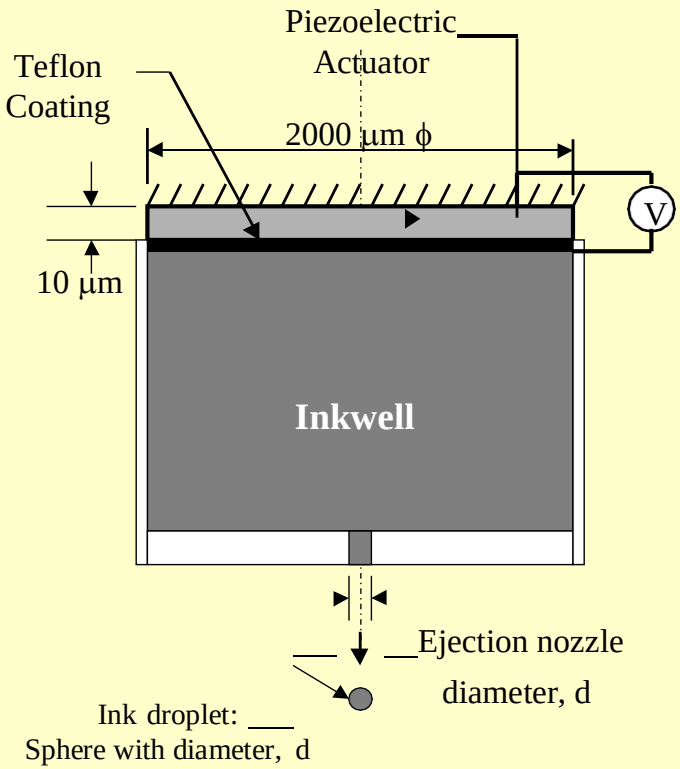

Let W = vertical expansion of the PZT cover induced by the applied voltage, V

Δ = diameter of the PZT cover = 2000 μm

We will have:

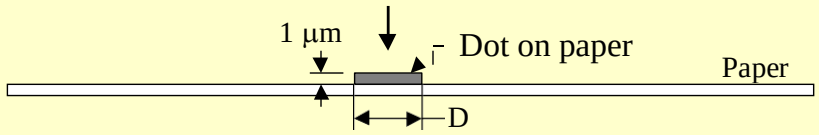

$$W = \frac{4V_{dot}}{\pi \Delta^2} = \frac{4x5629.21x10^{-18}}{3.1416(2000x10^{-6})^2} = 1791.83x10^{-12} \quad \text{m}$$

Example 7.5 – Cont'd

- **The corresponding strain in the PZT piezoelectric cover is:**

$$\varepsilon = \frac{W}{L} = \frac{1791.83x10^{-12}}{10x10^{-6}} = 179.183x10^{-6} \quad \text{m/m}$$

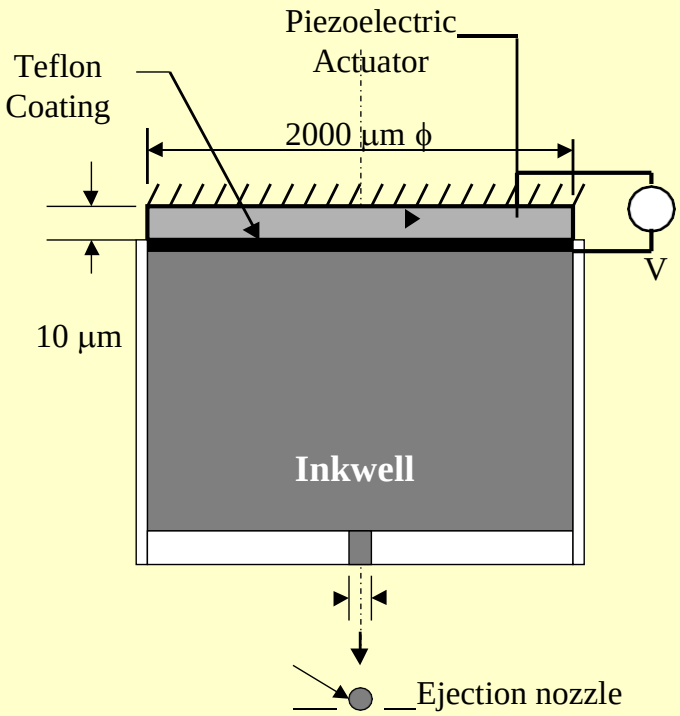

The piezoelectric coefficient of the PZT crystal is d = 480x10^{-12} m/v, leading to the **required voltage** to be:

$$V = \frac{\varepsilon}{d} = \frac{179.183x10^{-6}}{480x10^{-12}} = 0.3733x10^{6} \quad \text{volts/m}$$

or

$$v = LV = \left(10x10^{-6}\right)\left(0.3733x10^{6}\right) = 3.733 \quad \text{volts}$$

Polymers

What is polymer?

Polymers include: Plastics, adhesives, Plexiglass and Lucite.

Principal applications of polymers in MEMS:

- **Currently in biomedical applications and adhesive bonding.**
- **New applications involve using polymers as substrates with electric conductivity made possible by doping.**

Molecular structure of polymers:

- **It is made up of long chains of organic (hydrocarbon) molecules.**
- **The molecules can be as long as a few hundred nm.**

Characteristics of polymers:

- **Low melting point; Poor electric conductivity**
- **Thermoplastics and thermosets are common industrial products**
- **Thermoplastics are easier to form into shapes.**
- **Thermosets have higher mechanical strength even at temperature up to 350^{o}C.**

Polymers as industrial materials

Polymers are popular materials used for many industrial products for the following advantages:

- **Light weight**
- **Ease in processing**
- **Low cost of raw materials and processes for producing polymers**
- **High corrosion resistance**
- **High electrical resistance**
- **High flexibility in structures**
- **High dimensional stability**

Polymers for MEMS and microsystems

(1) Photo-resist polymers are used to produce masks for creating desired patterns on substrates by photolithography technique.
(2) The same photoresist polymers are used to produce the prime mold with desirable geometry of the MEMS components in a LIGA process in micro manufacturing.
(3) Conductive polymers are used as "organic" substrates for MEMS and microsystems.
(4) The ferroelectric polymers that behave like piezoelectric crystals can be used as the source of actuation in micro devices such as in micro pumping.
(5) The thin Langmuir-Blodgett (LB) films can be used to produce multilayer microstructures.
(6) Polymers with unique characteristics are used as coating substance to capillary tubes to facilitate effective electro-osmotic flow in microfluidics.
(7) Thin polymer films are used as electric insulators in micro devices, and as dielectric substance in micro capacitors.
(8) They are widely used for electromagnetic interference (EMI) and radio frequency interference (RFI) shielding in microsystems.
(9) Polymers are ideal materials for encapsulation of micro sensors and the packaging of other microsystems.

Conductive Polymers

- **Polymers are poor electric conducting materials by nature.**
- **A comparison of electric conductivity of selected materials are:**

Materials	Electric Conductivity, S/m*
Conductors:	
Copper, Cu	10^{6}-10^{8}
Carbon	10^{4}
Semiconductors:	
Germanium, Ge	10^{0}
Silicon	10^{-4}-10^{-2}
Insulators:	
Glass	10^{-10}-10^{-8}
Nylon	**10^{-14}-10^{-12}**
SiO_2	10^{-16}-10^{-14}
Polyethlene	**10^{-16}-10^{-14}**

* S/m = siemens per meter = Ω^{-1} = A^2-s^3/Kg-m^2

Conductive Polymers – Cont'd

Some polymers can be made electrically conductive by the following 3 methods:

(1) Pyrolysis:

Pyropolymer-base Phthalonitrile resin + **Amine** (at 600°C) = **Conductive polymer as high as 2.7×10^4 S/m**

(2) Doping:

Introducing metal atoms into molecular matrices of polymers

→ Conductive polymers

Polymers groups	Dopants
Polyacetylenes (PA)	Br_2, I_2, AsF_5, $HClO_4$ and H_2SO_4 for p-type Sodium naphthalide in tetrahydrofuran for n-type
Polyparaphenylenes (PPP)	AsF_5 for p-type; alkali metals for n-type
Polyphenylene sulfide (PPS)	AsF_5

(3) Insertion of conductive fibers:

Fibers made of Au, Ag, stainless steel, aluminum fibers and flakes.

Langmuir-Blodgett (LB) films

- The process was first introduced by Langmuir in 1917 and was later refined by Blodgett. That was why it is called Langmuir-Blodgett process, or LB films.

- The process involves the spreading volatile solvent over the surface-active substrate materials.

- The LB process can produce more than one single monolayer by depositing films of various compositions onto a substrate to produce a multilayer structure.

- LB films are good candidate materials for exhibiting ferro (iron)- , pyro (heat)- and piezoelectric properties. LB films may also be produced with controlled optical properties such as refractive index and anti reflections.

  They are thus ideal materials for micro sensors and optoelectronic devices.

Langmuir-Blodgett (LB) films – Cont'd

- **Following are a few examples of LB film applications in microsystems:**

(1) Ferroelectric (magnetic) polymer thin films:

- **The one in particular is the Poly-vinylidene fluoride (PVDF).**
- **Applications of this type of films include:**
  - **Sound transducers in air and water,**
  - **Tactile sensors,**
  - **Biomedical applications such as tissue compatibility, cardio-pulmonary sensors and implantable transducers and sensors for prosthetics and rehabilitation devices.**
- **As a piezoelectric source. The piezoelectric coefficient of PVDF is given in Table 7-14.**

(2) Coating materials with controllable optical properties:

- **Broadband optical fibers that transmit light at various wavelengths.**

Langmuir-Blodgett (LB) films – Cont'd

(3) Microsensors:

Many electrically conducting polymeric materials are sensitive to the exposed gas and other environmental conditions. So they are suitable materials for micro sensors.

Its ability of detecting specific substances relies on the reversible and specific absorption of species of interest on the surface of the polymer layer and the subsequent measurable change of conductivity of the polymer.

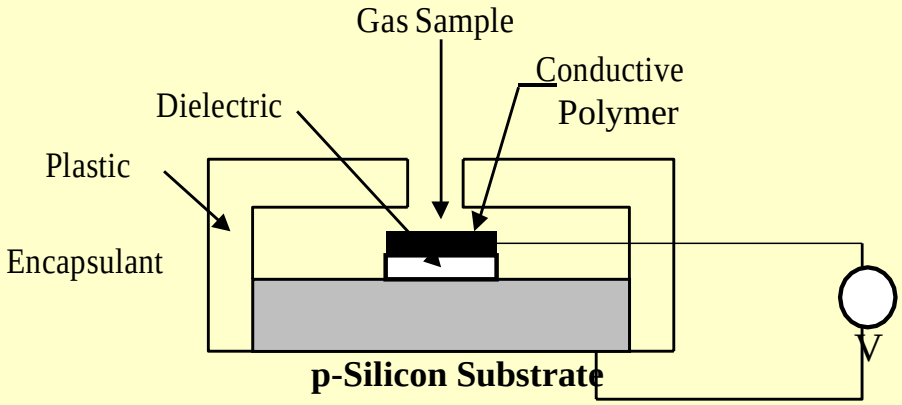

A gas sensor:

Electrical conductivity changes with absorption of the exposed gas.

SU-8 Photoresists

- It is a negative epoxy-based polymer sensitive to UV light (λ = 350-400 nm)
- It is used for thin-film production with thickness from 1 μm to 2 mm
- Reasons for it being popular in MEMS:
  - Can be built to thick films for 3-D MEMS structures (aspect ratio to 50)
  - Much lower production costs than thick films by silicon
- It is commercially available in liquid form
- SU-8 films can be produced by a spin-process:

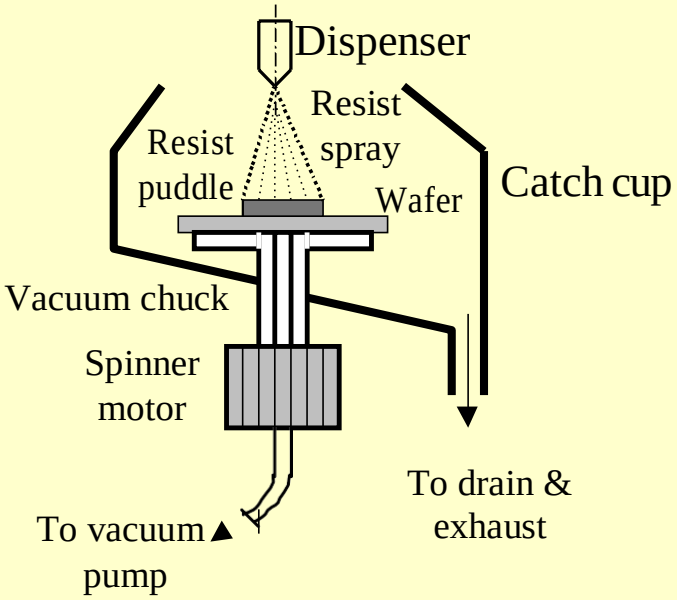

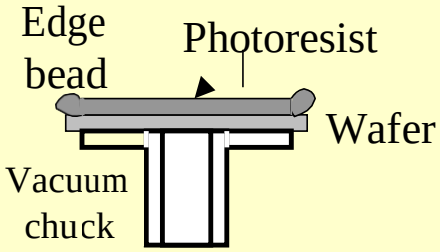

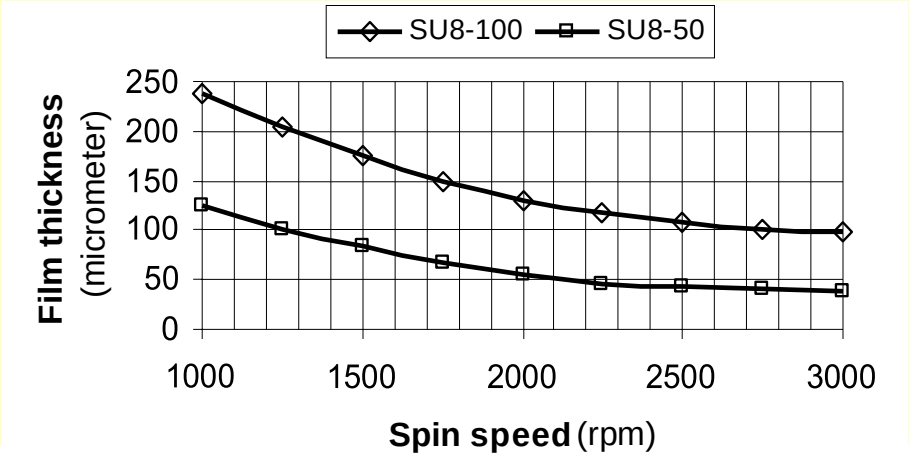

Mechanical Properties of SU-8 Polymer

Young's modulus	4400 MPa
Poisson's ratio	0.22
Viscosity	0.06 Pa-s (40% SU-8 – 60% solvent) 1.50 Pa-s (60% SU-8 – 40% solvent) 15.0 Pa-s (70% SU-8 – 30% solvent)
Coefficient of thermal expansion*	0.183 ppm /^{o}C
Thermal conductivity	0.073 W/cm-^{o}C
Glass transition temperature	200^{o}C
Reflective index	1.8 at 100 GHz 1.7 at 1.6 THz
Absorption coefficient	2/cm at 100 GHZ 40/cm a 1.6 THz
Relative dielectric constant	3 at 10 MHz

Source: Guerin 2005. * in comparison to 2.33 ppm/^{o}C for silicon

Typical Process Flow for Constructing SU-8 Films

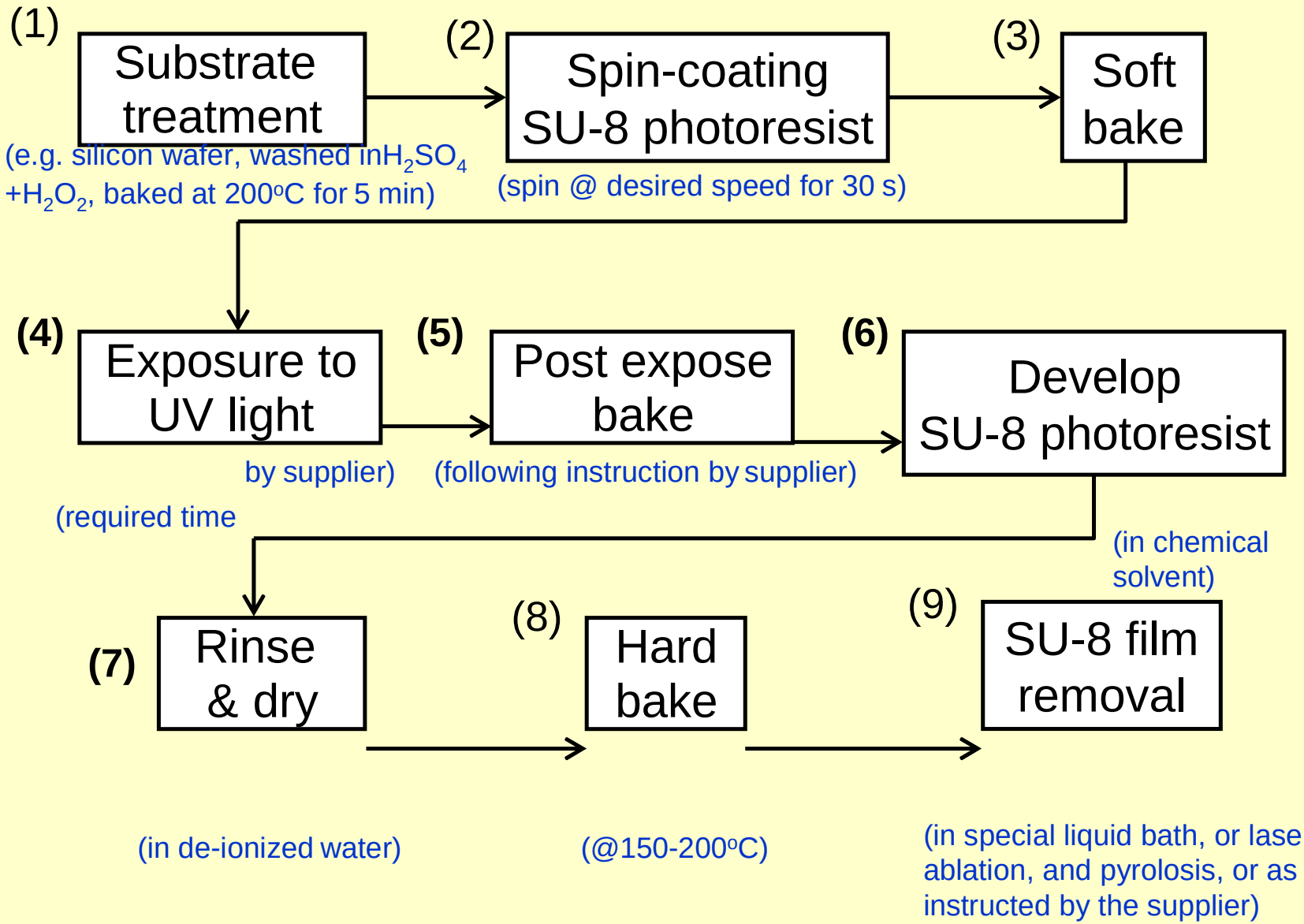

Packaging Materials

Unlike IC packaging in which plastic or ceramic are extensively used as encapsulate materials for the delicate IC circuits, MEMS packaging involve a great variety of materials-varying from plastic and polymers to stainless steel, as can be seen in a specially packaged micro pressure sensor:

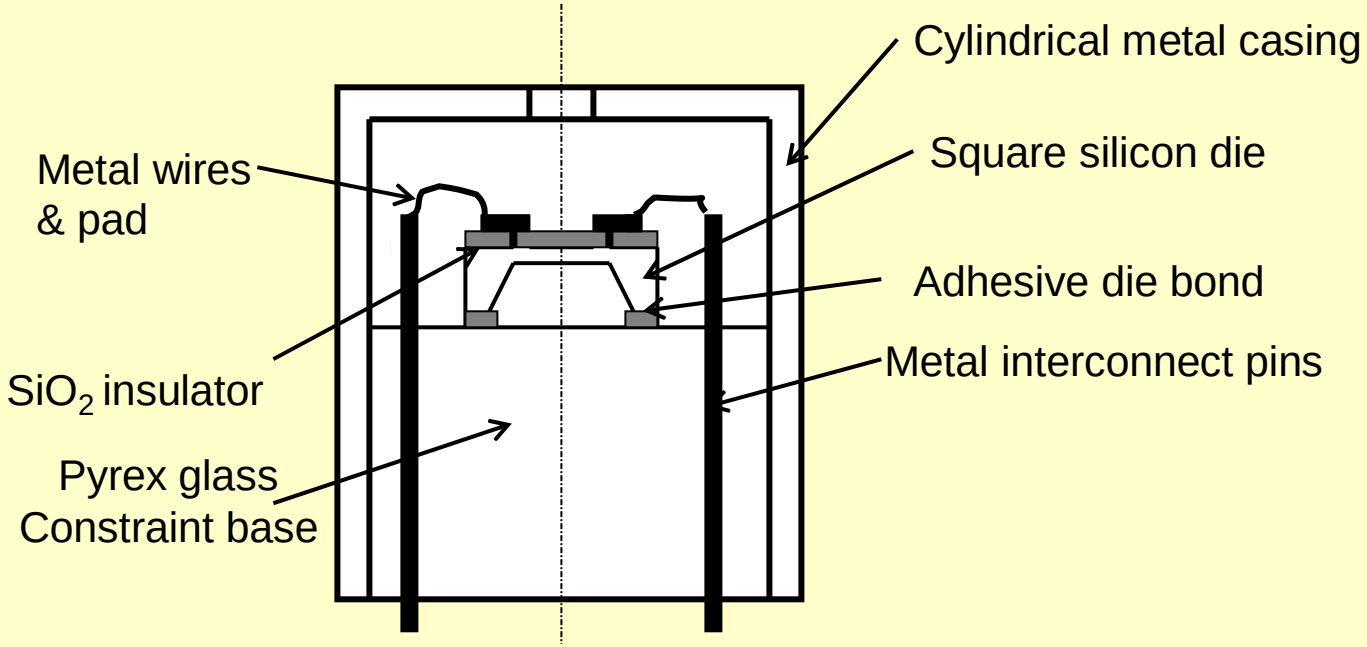

13.1 Introduction

We are on the threshold of a medical microdevice revolution that will change how we diagnose and treat patients. The promise of bioMEMs is the delivery of sensitive, selective, fast, low-cost, less invasive, and robust methods for diagnosis and pathogen detection. Individualized treatment directed at specific targets and genetic inadequacies will be made, as well as methods of therapy incorporating novel drug delivery devices and other actuator systems.

BioMEMs devices are to the future of medicine as microprocessors were to the computer revolution at the end of the last century, and of no less importance or potential impact. They are the platform upon which the human genome was sequenced in record time, and the basis for research of protein expression in health and disease. Likewise, they are the platform for performing point-of-service diagnostic testing and eventually monitoring evolution of disease in an individual and delivering customized nanomedicine therapy.

Microfluidic-based LOC devices and other μTAS, including DNA and protein microarrays, will be the basis of most if not all diagnostic tools within the next ten years. Transport of samples, reagents, and buffers through microfluidic systems based on electrokinetic and active pumping techniques will be at the heart of these systems. Actuator systems, including environmentally sensitive hydrogels, EAPs, and piezoelectric devices will be used for drug delivery systems, and to fabricate impressive biomimetic systems that imitate smooth and striated muscle function for future artifical muscles, hearts, diaphragms, and limbs.

Treatment-oriented devices will evolve more slowly, largely due to the infancy of the science, the need for confirming clinical studies, overcoming biocompatibility problems, packaging, safety, patent issues, and cost. Nevertheless, *they will evolve*, including both external and implanted systems.

In the beginning of the book I eluded to a future *Physician's Reference to Biomedical Devices* on the desk of every physician, and I hope the intervening chapters have convinced you of this possibility, and excited you into becoming involved in the revolution.

A number of applications have been cited in previous chapters to illustrate the principles and techniques discussed. Now we will look at a few more applications demonstrating integration of these techniques.

13.2 Minimally Invasive Surgery

BioMEMs devices in surgery may improve the functionality of existing surgical tools. They introduce new methodologies, and provide improved feedback or monitoring during procedures. Surgical considerations also include the implanting of probes, stimulators, and other bioMEMs devices such as the Reveal syncope sensor described below. Modification of an existing surgical tool may be advantageous for small companies developing bioMEMs devices, as lengthy clinical trials may be avoided if the modification does not alter the performance of the tool.

Minimally invasive surgery (MIS) is the process of accomplishing a surgical task with the least amount of intrusion, harm, and ultimately cost to the patient. There is typically less postoperative pain, shorter hospital stays, quicker recoveries and less scarring. Among the bioMEMs enhancement areas for MIS are tactile feedback, tissue sensing, and tracking systems [Rebello, 2004].

For example, fiberoptic instruments and small tools may be used to remove a gallbladder through small holes in the abdomen rather than the traditional open incision. Recovery time is markedly improved, and ultimately the risk is lessened (in the hands of a surgeon experienced with the procedure, and with proper choice of technique). The downside is less visualization and "hands-on" mobilization of organs, and some increased risk of bleeding or other complication that may require ultimately converting to an open procedure. MIS accounts for 40% of procedures, and is projected to increase to 80% in the next 15 years [Rebello, 2004].

13.3 Point-of-Care Clinical Diagnosis

Combining microfluidic devices, detection schemes, and microarray devices is the natural evolution for μTAS systems. Advantages of integrated chips include low sample/reagent volume, rapid analysis time, less sample wastage, cost effectiveness, and potential for disposability. Microfluidic systems may be active or passive devices. Advantages of a passive system include no need for a power system, ease of integration, continuity in substrate material, rapid prototyping, low cost, and use without active control. Passive microfluidic components, including valves, mixers (including diffusion), filters, and membranes, were discussed in Chapter 5. Active systems require a reliable power source (typically battery power for hand-held systems) and control electronics. Another consideration for an integrated system is choosing the best substrate, including silicon, glass, or polymer materials.

A disposable smart plastic fluidic biochip for clinical diagnosis is shown in Fig. 13.1. This cartridge-like device and supporting electronics is quite novel in its level of integration. Figure 13.2 shows schematically the passive microfluidic manipulation system based on the *structurally programmable microfluidic system* (sPROMs) technology developed by Ahn et al. (2004). The novelty of this device is that it allows for a preprogrammed set of microfluidic sequencing with only an on-chip pressure source. The integration of an air-bursting detonator is the fluid-driving source, eliminating the need for active microfluidic pumps. An integrated biosensor array is included for simultaneous detection of multiple clinically relevant parameters. The biochip is inserted into the analyzer unit, where the microfluidic sequencing is initiated by a trigger signal from an electronic controller. After the sample solution (blood) is delivered to the biosensor array, the electrochemical detection circuitry on the analyzer is used to determine the concentrations of the various analytes.

COC was used for the substrate. A custom designed Ni molding block was produced by microfabrication. A rapid thermal process of injection molding was used. The surface of the Ni mold was heated with IR radiation to the same temperature as the injected polymer, which minimizes heat transfer on injection and allows for better flow into the mold detail (Fig. 13.3).

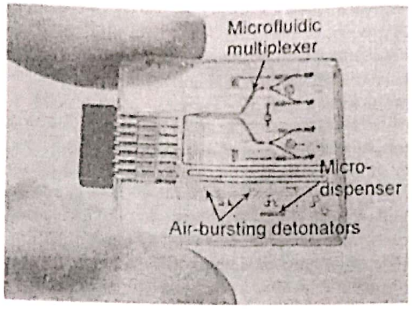

Figure 13.1 Assembled biochip with sPROMs-based microfluidic control system and air-bursting detonators for fluid driving. [Reprinted with permission from Ahn et al. (2004), copyright IEEE.]

In this device microfluidic manipulations are carried out in a *preprogrammed sequence* without the need for an external control signal. Figure 13.4 shows schematically the integrated dispenser. The reservoir is filled and fluid dispensed in a precise manner through a tree of microchannels (1–7). Flow is controlled with microvalves (R_1–R_6) and channel geometries.

The passive microvalve operates on the principle that when an abrupt change in width is effected across a microchannel fabricated on a hydrophobic substrate, a substantial pressure would be needed to push the fluid across the

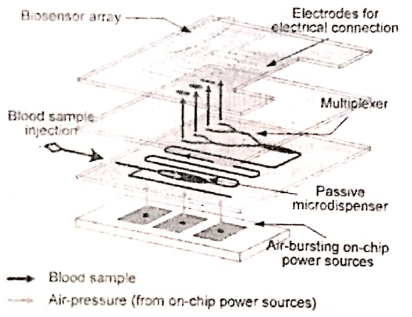

Figure 13.2 Schematic illustration of multianalyte detection disposable biochip cartridge. The biochip incorporates on-chip power sources for passive microfluidic manipulation and a biosensor array for blood analysis. [Reprinted with permission from Ahn et al. (2004), copyright IEEE.]

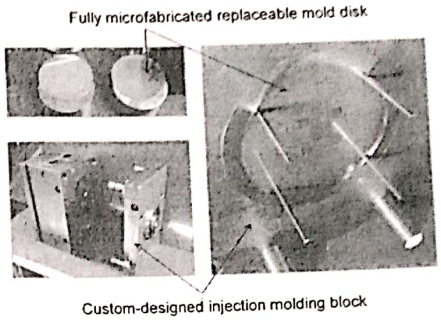

Figure 13.3 Photographs of the custom designed molding block with the replaceable Ni mold disk and the fabricated microstructures in the Ni mold disk insert. [Reprinted with permission from Ahn et al. (2004), copyright IEEE.]

restriction. The pressure required to move the fluid into the channel before the passive valve is expressed by the Hagen-Poiseuille equation for a rectangular channel:

$$\Delta P_1 = \frac{12L\mu \cdot Q}{wh^3},$$

where

L is the length of the channel,
μ is the viscosity of the fluid,
Q is the flow rate,
w is the width of the channel, and
h is the height of the microchannel.

The pressure required to overcome the passive valve (to overcome surface energy of the narrow channel derived from the higher surface-area-to-volume

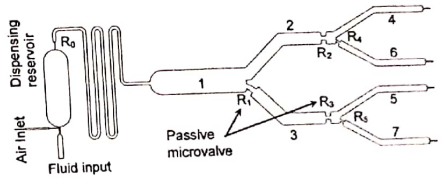

Figure 13.4 Microfluidic multiplexer with integrated dispenser used to demonstrate the sPROMs concept. [Reprinted with permission from Ahn et al. (2004), copyright IEEE.]

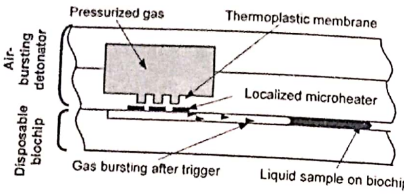

Figure 13.5 Schematic drawing of the disposable air-bursting detonator as an alternative on-chip power source. [Reprinted with permission from Ahn et al. (2004), copyright IEEE.]

ratio) is calculated as

$$\Delta P_2 = 2\sigma_l \cos(\theta_c)\left[\left(\frac{1}{w_1} - \frac{1}{h_1}\right) - \left(\frac{1}{w_2} - \frac{1}{h_2}\right)\right],$$

where

w_1 and h_1 are the width and height of the channel before the obstruction,
w_2 and h_2 are the width and height of the channel after the obstruction,
θ_c is the contact angle of water with the hydrophobic surface, and
σ_l is the surface tension.

If the depth is constant (more easily accomplished with micromachining), and h_1 equals h_2, then the pressure above is

$$\Delta P_2 = 2\sigma_l \cos(\theta_c)\left[\left(\frac{1}{w_1} - \frac{1}{w_2}\right)\right].$$

Air-bursting detonators consist of pressurized gas stored in on-device chambers and released via an electronic pulse to heater. The heater may be used to either melt a polymer seal or create thermo stress in a sealing membrane, releasing the gas to drive fluids through the channel. Figure 13.5 shows this concept schematically.

Detection of oxygen is accomplished with amperometric detection as depicted in Fig. 13.6. Electrode-design modification allows for lactose and glucose sensing as well. The sPROMs cartridge and supporting electronics assembly are shown in Fig. 13.7. Use of application-specific integrated circuits (ASICs) may allow further reduction of the electronics package size.

13.4 Cardiovascular

13.4.1 Introduction

Biomedical devices for cardiovascular uses have a long and established history, including use of extracorporeal circulation for open-heart surgery, pacemakers,

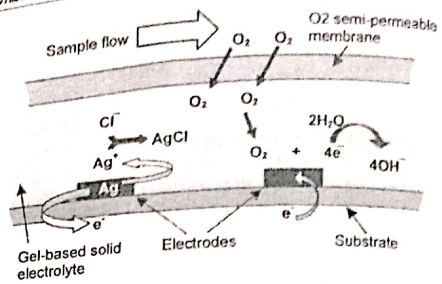

Figure 13.6 Electrochemical and analytical principle of the developed biosensor for partial oxygen concentration sensing. [Reprinted with permission from Ahn et al. (2004), copyright IEEE.]

implantable defibrillators, artifical hearts, left-ventricular-assist devices, and artificial-vascular-grafting material. Numerous catheter devices have also been developed for angiography, angioplasty, stent placement, measuring cardiac performance, intravascular feeding, inferior-vena-cava-umbrella placement to prevent pulmonary embolism in deep venous thrombosis, intra-arterial catheters for opening blocked peripheral arteries, and intra-aortic balloon-assist devices for cardiac failure.

The next generation of cardiovascular devices will be based on bioMEMs, and will include surface modifications and treatments of implanted devices, and catheters to minimize clotting and improve biocompatibility. Microsensors will be used for measuring pressure, flow, and other parameters, and microactuators will affect immediate responses.

Automatic sensing of problems and taking preemptive action will be the new patient management paradigm. Many bioMEMs devices will be wireless and will not require on-board power sources. Devices may be directly implanted

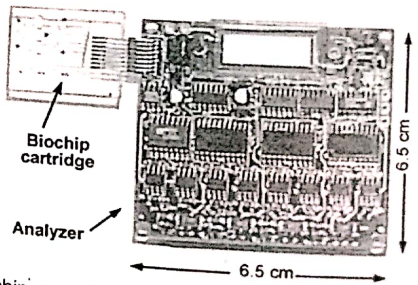

Figure 13.7 Biochip cartridge is inserted into an analyzer module for detection. [Reprinted with permission from Ahn et al. (2004), copyright IEEE.]

into the heart and other organs, and with appropriate feedback and drug-delivery systems they will revolutionize treatment of congestive heart failure, myocardial ischemia, and arrhythmias.

13.4.2 Pressure and flow measurement

In 1998, Kalvesten et al. produced the first surface micromachined pressure sensor for commercialized blood pressure measurements. A silicon chip with a diaphragm and a piezoresistive pressure sensor measured blood pressure accuracy better than 2 mm/Hg. This pressure sensor is used clinically for blood pressure measurements in balloon angioplasty applications.

A catheter-based intracardiac ultrasound that offers the potential for improved guidance of interventional cardiac procedures has been proposed [Zara et al., 1999]. The forward-looking mechanical sector scanner incorporates high-frequency ultrasound transducers operating at frequencies up to 20 MHz by using PZT devices mounted on a polyimide table that pivots on gold-plated polyimide hinges. This table-mounted transducer is tilted using a linear MEMS actuator to produce a sector scan. The prototype transducer/actuator assembly was fabricated and interfaced with a personal computer to create a single channel ultrasound scanner. A newer design uses ANSYS finite-element software to maximize the sector-scan angle for the forces produced by the linear actuator, the integrated force array (IFA) [Zara et al., 2000]. The design includes both a forward-looking hinged table similar to the previous prototypes and a new side-viewing device that has a transducer table tilting on miniature torsion hinges.

A wireless flow probe for intravascular flow measurement has been developed [Takahata et al., 2004]. A dual-inductor antenna stent consisting of helical coils and capacitors form an LC circuit (impedance-capacitance) system. No battery is required for operation. The device is fabricated from 50-μm thick stainless steel foil by using batch-compatible micro-electro-discharge machining (EDM). Two capacitive pressure sensors are microfabricated and incorporated into the device. To demonstrate the probe the device is deployed inside a silicone mock artery with a standard angioplasty balloon. The planar structure is plastically deformed to a tubular shape, resulting in dual helical coils of 50–60 nH (nano-Henry) impedance each. These LC tanks are used to wirelessly probe pressures at two points along a channel for flow-rate detection. Fluidic experiments that emulate a blockage in the mock artery demonstrate that the resonant impedance and phase provided by the LC-tanks to a separate transmitting coil shift by 5–40 MHz over a flow-rate change of 150–300 mL/min. Pressure sensitivity is 273 ppm/Torr, which is one hundred times higher than past results.

A variety of other techniques for navigation systems, sensors, and actuators for catheters and endoscopes and other minimally invasive techniques are reviewed by Haga and Esashi (2004).

13.4.3 Cardiac muscle function

A bioMEMs force transducer system has been developed to measure forces generated by living heart muscle cells *in vitro* to better understanding muscle contraction. Cell attachment and measurement of contractile forces have been demonstrated with a commercially fabricated surface-micromachined hinged polysilicon device. Two freestanding polysilicon clamps, each suspended by a pair of microbeams, hold each end of a heart cell. When the cell contracts, the beams bend and force is determined from the measured deflection and the spring constant in the beams [Lin et al., 2000].

13.4.4 Syncope assessment

The Medtronic Reveal is an implantable device for monitoring *syncope*, the sudden loss of consciousness (Fig. 13.8). The device can monitor the cardiac rhythm for up to 14 months, and records symptoms or abnormalities in real time. The patient may activate recording with an external triggering device. A doctor uses another device to download the data. It is easy to use and there are no connections to come loose, but requires a surgical procedure for implantation. Ultimately it helps to differentiate cardiac versus neurological causes for syncope, and may detect intermittent atrial fibrillation.

A flowchart of the strategy for evaluating the syncopal patient is shown in Fig. 13.9. As an adjunct to the cardiovascular workup, the Reveal unit assists in excluding underlying cardiac arrhythmia as the cause. The diagnostic yield for traditional methods is shown in Fig. 13.10.

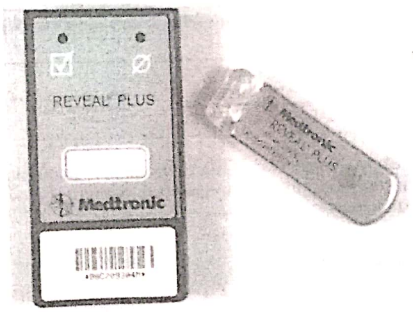

Figure 13.8 The Medtronic Reveal Plus external interface (left) and the implanted unit (right). A separate system at the physician's office is used to download the data. (Image Courtesy of Medtronic.)

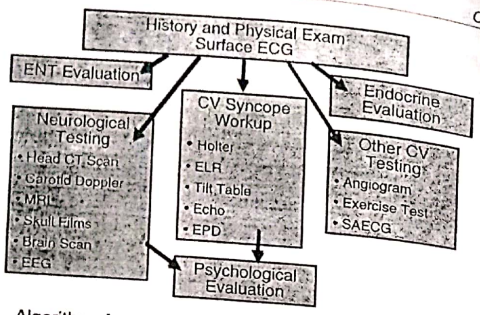

Figure 13.9 Algorithm for distinguishing the various causes of unexplained syncope, or loss of consciousness. (Image courtesy of Medtronic.)

Test/Procedure	Yield	Monitoring Duration
History & Physical	49-85%[1,2]	NA
ECG	2-11%[2]	15 minutes
Holter Monitor	1%*	1-3 days
Electrophysiology Study without SHD**	11%[3]	NA***
External Loop Recorder	20%*	2-3 weeks
Tilt Table Test	11- 87%[4,5]	NA***
Electrophysiology Study with SHD**	49%[3]	NA***
Reveal Insertable Loop Recorder	65 - 88%[6,7]	Up to 14 months

et al *N Eng J Med*, 1983.
Am J Med, 1991.
et al. *Ann Int. Med*, 1997.
Medicine, 1990.
[5] Kapoor, *JAMA*, 1992
[6] Krahn, *Circulation*, 1995
[7] Krahn, *Cardiology Clinics*, 1997.
* Yield based on mean time to diagnosis of 5.1 months[7]
** Structural Heart Disease
*** Provocative test

Figure 13.10 Conventional diagnostic methods for diagnosing the cause of syncope, diagnostic yield, and time required to perform the evaluation. (Image courtesy of Medtronic.)

13.5 Diabetes

13.5.1 Continuous glucose monitoring

Accurate, continuous glucose monitoring can improve diabetic patient care, providing early warning of hypoglycemia or hyperglycemia, and may be useful for

control of insulin pumps. An upgrade to multiparameter monitoring would not only benefit patients with severe metabolism defects but also the metabolism of diabetes patient could be better controlled by monitoring an additional parameter like lactate [Moser, 2003].

Unfortunately, one of the complications in the integration of different biosensors using the same detecting molecule for all analytes is chemical cross talk between adjacent amperometric biosensors. These issues and others for clinical diagnosis implementation are reviewed by Moser (2003).

13.5.2 Microdroplet analysis

Srinivasan et al. (2004) use a different approach to measure glucose *in vitro* based on microdroplet analysis on a LOC device. The droplets act as solution-phase reaction chambers and are manipulated using the *electrowetting* effect. Electrowetting refers to the modulation of the interfacial tension between a conducting liquid phase and an insulated solid electrode, by the application of an electric potential between the two.

Figure 13.11 shows a vertical cross section of the electrowetting chip along with the optical detection instrument. The electrowetting system consists of two parallel glass plates separated by a spacer of known thickness. The bottom plate consists of an array of electrodes that are independently addressable (patterned on indium-tin oxide). The top plate serves as the ground electrode, and both plates are coated with Parylene and Teflon. Droplets of the glucose sample are pipetted manually onto the electrowetting chip. Mixing occurs by moving the coalesced droplet across three electrodes for 15 s by application of 50 V at 8 Hz. Once mixed, absorbance is measured over 30 s by holding the droplet stationary. Glucose is measured using a colorimetric enzyme-kinetic method based on Trinder's reaction. The color change is detected using an absorbance measurement system consisting of a light-emitting diode and a photodiode [Fair et al., 2003; Srinivasan et al., 2004].

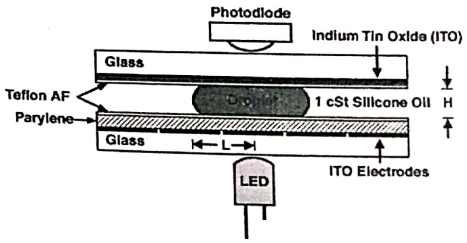

Figure 13.11 Vertical cross-section of the electrowetting setup along with the optical absorbance measurement instrumentation. [Reprinted with permission from Srinivasan et al. (2004), copyright McGraw-Hill.]

13.6 Endoscopy

13.6.1 Introduction

Endoscopy includes the process of passing a fiber optic tube through either the upper or lower gastrointestinal tract to visualize inside and perform procedures. On one end of the instrument are an objective lens and a camera for seeing and recording, on the other end are a flat optical surface and a light source. Other channels may exist in the tube for passing instruments.

Other similar fiber optic visualization includes arthroscopy for looking into joints, bronchoscopy for looking into the lungs, mediastinoscopy for looking at the chest mediastinum, laparoscopy for looking at internal organs through the abdominal wall, and hysteroscopy for looking into the uterus. Flexibility and control of the tip of the instrument, image quality, size, and the ability to work through the instrument (biopsy, cauterize, and other surgery) are all important facets of the process.

13.6.2 Optical coherence endoscopy

Boas (2003) describes an electrostatically controlled scanning mirror for OCT for endoscopy. Movement of the mirror is accomplished by an integrated force array of hundreds of thousands of micron-scale capacitors that, when voltage is applied across their electrodes, contract and pull the mirror directionally.

Goa et al. [1998(a) and (b)] describe a micromotor control for the front tip of an endoscope.

13.6.3 Micro-optical scanner

Seibel et al. (2003) describe development of a micro-optical scanner at the tip of an ultrathin flexible endoscope with an overall diameter of 1 mm. Through the use of a piezoelectric tube actuator with a small diameter, a cantilevered optical fiber can be driven in mechanical resonance to scan a beam of light in a space-filling, spiral-scan pattern.

Figure 13.12 shows the diffuse lighting from a standard flexible endoscope (top); a scanning point source (middle), and a microlensed optical fiber scanner (bottom), creating a directed beam of illumination that is focused with a lens.

By knowing and/or controlling the fiber position and acquiring backscattered intensity with a photodetector, an image is acquired. Micromachining is used to create the small diameter optical fiber, and a microlens (less than or equal to 1 mm in diameter) is fabricated on the end of the fiber. The mass and location of the lens cause the microlens to undergoing angular rotation along two axes with minimal lateral microlens displacement. Other mirror systems have been described by Xie et al. (2003), and Zara et al. (2003).

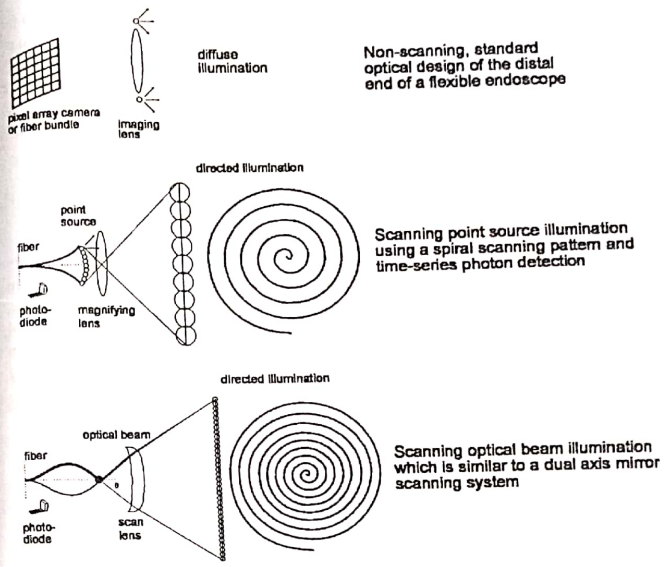

Figure 13.12 Top functional diagram depicts current technology that uses diffuse illumination, imaging lenses, and a pixel-array for image transmission and capture (coherent fiberoptic bundle or camera). Middle level depicts the distal end of an optical fiber that creates a point source and scans across an object plane, imaging out to the magnified illumination plane. The proposed opto-mechanical design is depicted in the bottom level with a microlensed optical fiber scanner creating a directed beam of illumination that is focused with a scan lens. In the two fiber-scanning embodiments, the backscattered light is detected with a single RGB photodetector, but light can be collected by the same optical fiber in a confocal arrangement (Seibel, 2003).

13.7 Neurosciences

13.7.1 Introduction

Neurology, neurosurgery, and related research comprise the neurosciences. Neural prosthesis, intracranial-pressure-monitoring (ICP) systems, smart ICP management systems, biochemical, and physiological brain and spine monitoring systems, microsurgical tools, drug-delivery systems, tissue engineering, and

molecular biology techniques are applications envisioned by Roy et al. (2001) for neurosurgery. Among the systems reviewed by the authors, the incorporation of pressure sensors, strain gauges, and biochemical sensors in surgical instruments (*smart tools*) are included; as are micromachined probes, and cutting tools for greater precision and performance; implanted pressure and strain sensors for continuous spinal fusion assessment (Fig. 13.13); and neural regeneration devices (Fig. 13.14).

13.7.2 Probes

Flexible-probe arrays that may be placed in the brain for measuring neural activity at different levels have been described by Stieglitz and Gross (2002) and Takeuchi et al. (2004). Figure 13.15 shows the fabrication process of one of these devices, where nickel is electroplated on a silicon wafer, polyimide is spin coated and metal layers are deposited, patterned, and spun again to cover the metal layer. Oxygen plasma is used to pattern the polyimide, the silicon is DRIE etched, and residual silicon is removed from the backside by XeF_2. The probes are then folded. The final device with interconnections is seen in Fig. 13.16.

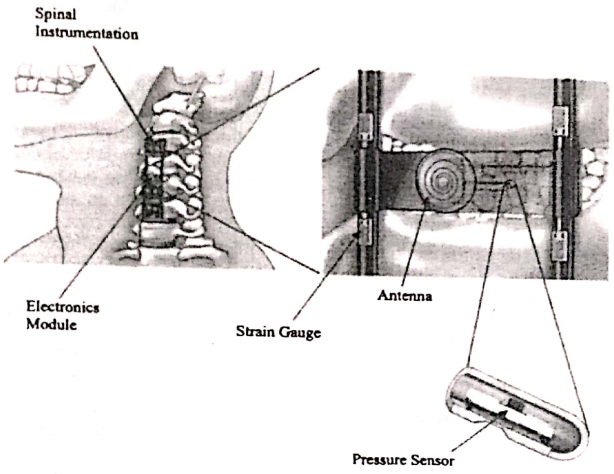

Figure 13.13 Schematic depiction of an implantable fusion assessment system using MEMS pressure sensors and strain gauges. The strain gauges monitor loads on the instrumentation, and the pressure sensor is used to assess pressure within the bone graft. The measured pressure and load information is transmitted to an external receiver via wireless telemetry. [Reprinted with permission from Roy et al. (2001), copyright Lippincott, Williams, and Wilkins.]

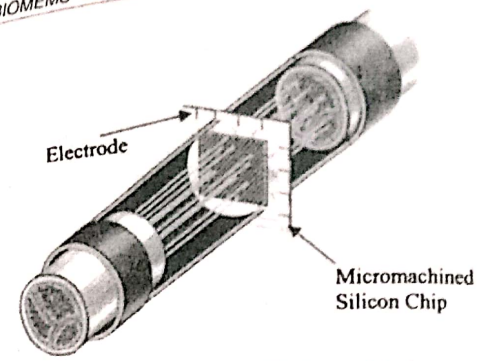

Figure 13.14 Schematic depiction of a MEMS-based device neural regeneration interface. The perforated silicon chip spatially constrains growing ends of the nerve fibers in close proximity. Additional electrodes are incorporated for possible recording and stimulation. [Reprinted with permission from Kovacs et al. (1992), copyright IEEE.]

Development of a high-density electronic interface to the central nervous system by fabrication of an electrode array was demonstrated by Wise et al. (2004). This remarkable work engages many of the problems associated with implantable medical devices, including integrated CMOS circuitry and probes; sensing, stimulation, and drug delivery through the probes, miniaturization and packaging for biocompatibility; and wireless inductive RF telemetry. Many implementations of the technology are described in the work. For example, Fig. 13.17 shows a 64-site, 8-channel stimulating probe (multiple sensors are along each tangent); and Fig. 13.18 shows the sensor multiplexing scheme for data flow. A block diagram of an inductive RF telemetry link is shown in Fig. 13.19. Three-dimensional assembly of these probes into arrays permits the ability to sense or stimulate every cell within a block of tissue while displacing less than 1% of the volume.

Implantable *neuroprobe* systems that have closely integrated chemical and electrical neural interfaces have also been developed [Kipke, 2003]. The neuroprobe consists of a silicon or polymer substrate with multiple metal sites for electrical recording and/or stimulation and one or more microchannels for fluid delivery. A *chronoamperometric* chemical sensor is achieved by selectively coating metal sites with an ion-selective membrane. This system provides a technology for establishing chronic and controllable chemical and electrical interfaces to targeted areas of the brain and spinal cord.

13.7.3 Nerve regeneration

Peripheral nerve injury affects 2.8% of trauma patients and can be very disabling. When a peripheral nerve is transected, *Wallerian degeneration* occurs in all of the

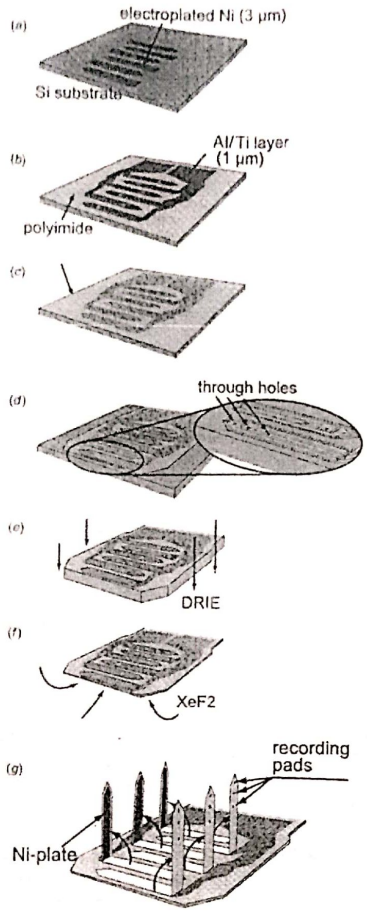

Figure 13.15 Fabrication process of the flexible-probe array: (a) nickel is electroplated on a silicon wafer; (b) polyimide is spin coated and metal layers are deposited and patterned; (c) polyimide is spin coated again to cover the metal layer; (d) oxygen plasma is used to pattern the polyimide; (e) the silicon is DRIE etched; (f) residual silicon is removed from the backside by XeF_2; and (g) the probes are folded. [Reprinted with permission from Takeuchi et al. (2004), copyright Institute of Physics.]

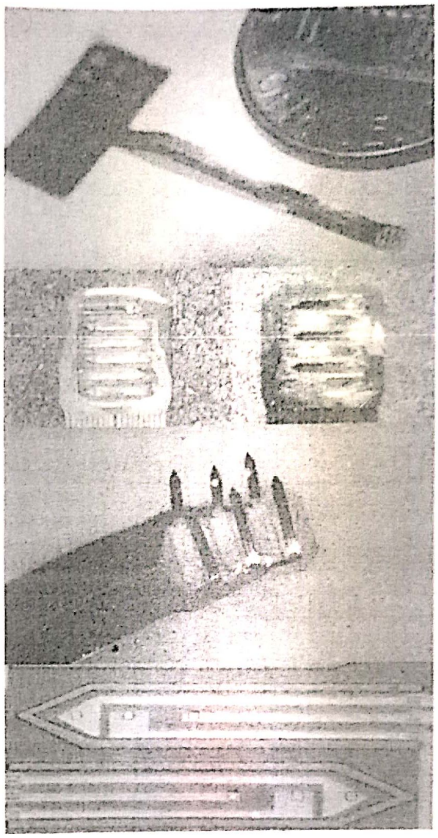

Figure 13.16 Finished flexible probe array. [Reprinted with permission from Takeuchi et al. (2004), copyright Institute of Physics.]

axons distal to the injury site. This occurs because the nerve axon is separated from the cell body located in the spinal cord, dorsal root ganglia, or autonomic ganglia. Once severed, the distal nerve does not receive necessary nutrition and degenerates within days. Myelinated and unmyelinated fibers at some distance proximal to the injury spontaneously sprout new axons. These occur at the node of Ranvier.

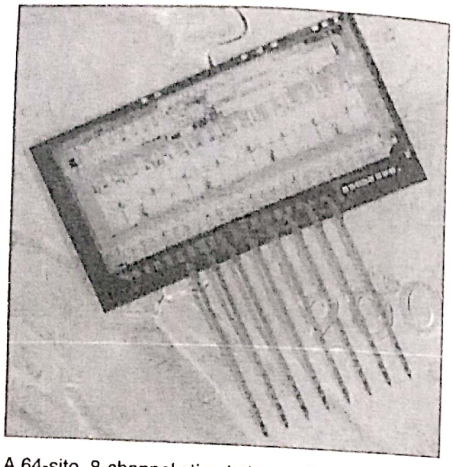

Figure 13.17 A 64-site, 8-channel stimulating probe on a U.S. penny. [Reprinted with permission from Wise et al. (2004), copyright IEEE.]

The regenerating segments may reach their intended target by preferential stimulation, but do not necessarily do so.

The goal of nerve repair is to direct the regenerating nerve fibers into the proper distal endoneurial tubes that lead the regenerating axons to the appropriate end organ. In spite of advances in the technology, to date no tubular or other type of conduit has proved superior to the autologous nerve graft [Belkas et al., 2004].

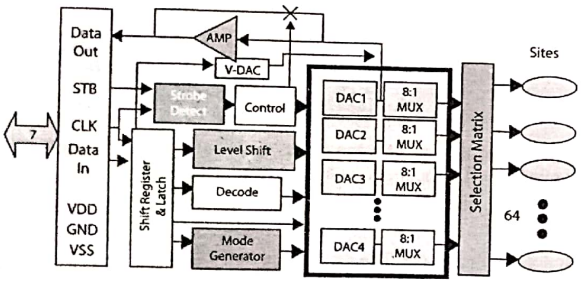

Figure 13.18 Schematic diagram of the microcontroller interface and stimulating probe output. A serial input data stream controls the current amplitudes present at each probe. [Reprinted with permission from Wise et al. (2004), copyright IEEE.]

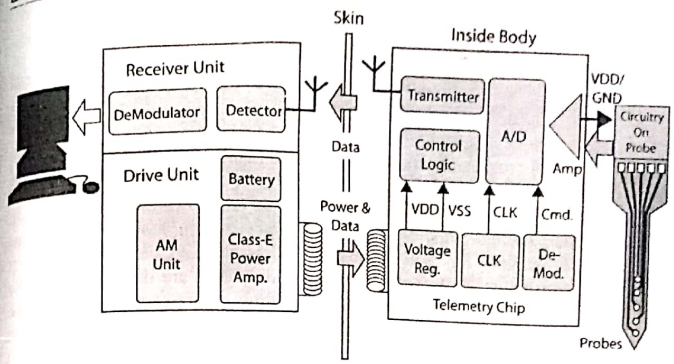

Figure 13.19 Block diagram of an inductive RF telemetry link for an implantable microsystem (more on this in Chapter 14). [Reprinted with permission from Wise et al. (2004), copyright IEEE.]

13.8 Oncology

13.8.1 Introduction

Cancer arises because of abnormal DNA mitosis that results in uncontrolled proliferation of cells with altered function, and often with the ability to metastasize, or spread to other parts of the body. This may occur by direct extension (invasive), or through the lymphatic or vascular systems. Cancer kills primarily by its physical and hormonal interruption of normal organ function. For example, colon cancer may cause bowel obstruction or motility problems, as well as interfere with normal ventilation by producing pulmonary effusions that limit lung expansion or promote development of infection. Some lung cancers secrete hormones that may cause fatigue and muscle weakness. Loss of appetite and weight loss commonly occur with cancer.

Current cancer therapy is dependent on the type and histology of the cells, and established protocols. National protocols allow consistency in treatment and ability to analyze therapy based on group responses through statistical analysis. Since therapy is usually investigational per se, it would not be practical for every oncologist to use totally different treatment methods, but rather to pick from approaches currently showing the most promise. Certain study drugs, however, may be only available to a limited subset of investigators; hence, a limited number of patients may be receiving a specific treatment. Cancer detection includes mammography, x-rays, nuclear-isotope scans, CT scans, MRI scans, and PET scans (see Appendix B).

13.8.2 High-throughput screening

High-throughput screening of tumor cells based on rapid protein synthesis and mitosis characteristic of cancer cell proliferation has been accomplished by Gourley et al. (2000). Traditionally, cells are analyzed by preparing tissue sections and stained slides from which a pathologist may study the cellular morphology. Another approach proposed by the authors is to evaluate tumor cells by quantifying their growth kinetics. *Nanolasers* are very small laser devices, often smaller than the wavelength of the light they produce. The lasers have been used to distinguish cancerous from normal cells. Cells made to flow through a microfluidic laser cavity can be analyzed for protein content. This is accomplished by looking at spectral shifts in the lasing frequencies as individual cells are illuminated by the coherent light beam. Compared to traditional flow cytometers, such a device may analyze samples as they are drawn from a patient, or conceivably could be incorporated into a scalpel for immediate determination of a cancer resection with tumor-free edges (resecting all of the affected tissue).

The detection of autoantibodies to tumor antigens has potential utility for the early diagnosis of cancers. Microarrays provide high throughput and high sensitivity alternative to the use of Western blots for tumor antigen profiling. Microarrays of tumor-derived proteins provide the means for uncovering many tumor antigens that have induced an antibody response in patients with specific cancers [Qiu et al., 2004].

Molecular beacons have been used in a biochip for analysis of the breast cancer gene BRCA1 [Culha et al., 2004], and a low-density DNA microarray for analysis of markers in breast cancer has been developed [Lacroix et al., 2002].

A combined DNA and protein probe chip may be used to detect the tumor suppressor gene fragile-histidine triad (FHIT). Detection of FHIT gene is important in cancer diagnostics since its alterations have been associated with several human cancers [Askari et al., 2002].

13.9 Ophthalmology

13.9.1 Introduction

The back of the eye, upon which light is focused, is known as the retina. Light is sensed by the rods and cones of the retina and communicated to the occipital lobe of the brain via the optic nerve. Figure 13.20 shows the composition of the retina, including the neural layers that are in front of the photoreceptors. The methods by which information is encoded in the optic nerve, and the decoding and interpretation in the brain are unknown. Researchers are using bioMEMs devices to emulate the light-retina interface (epiretinal and subretinal space) in hopes of directly stimulating the retina surface with an image. This may prove useful for some patients with retinal disease.

In addition to the cornea, lens, and controlling musculature, the eye also contains a clear vitreous material through which light travels. Elevation of the

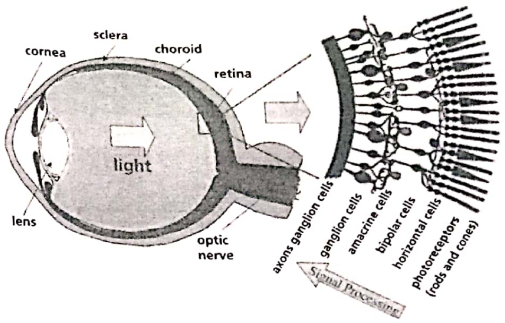

Figure 13.20 Light passes through the eye and through the neural layers of the retina before reaching the photoreceptors. [Reprinted with permission from Meyer (2002), copyright Elsevier.]

intraocular pressure is known as glaucoma, and is typically treated with either surgical procedures or medication.

Retinitis pigmentosa is a group of inherited diseases that affect the retina by causing degeneration of the photoreceptor cells (cones and rods). Loss of night vision and loss of either peripheral vision (primarily rod-cell degeneration) or central vision (rod-cone dystrophy) are common initial manifestations.

13.9.2 Retinal implants

Two types of ophthalmologic implants, one for continuous measurement of intraocular pressure in glaucoma patients; and the other for epiretinal stimulation of the nerve cells of the retina to assist patients with retinitis pigmentosa, receive visual response from their environment as described by Mokwa (2003).

Future high-resolution retinal prosthesis devices require a method for interconnecting an imaging system to the retina [Peterman et al., 2002]. Such a system must be able to individually address and stimulate retinal neurons. Peterman et al., produced an electronic-to-biologic interface using microfabricated apertures in a silicon substrate. Apertures are created in a thin silicon-nitride membrane, after which the surface is appropriately modified to support cell growth. Cells that can be excited with stimulation and imaged with fluorescent dyes cover the membrane. The device has been demonstrated to coat cells at precise locations.

A micromachined conformal electrode array that conforms to the topography of the retina has been developed by Okandan et al. (2003). Individual electrodes

are located on micromachined springs that float on a substrate. Spring constants (contact force) are adjusted when the dimensions of the springs at each electrode are adjusted.

Kolnsberg et al. (1999) described an epiretinal system consisting of three functional units: a CMOS image sensor and encoder (worn like a pair of eyeglasses), a telemetry unit (external transmitter and internal receiver), and a flexible retinal substrate (Fig. 13.21). The microelectrode array on an ultra-thin LI substrate is shown at two magnifications in Fig. 13.22. A photograph of the finished assembly

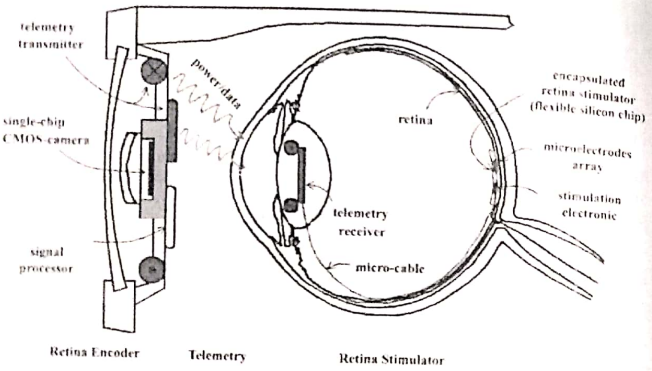

Figure 13.21 Epiretinal system consisting of three components: (1) CMOS image sensor and encoder; (2) telemetry unit (external transmitter, implantable receiver); and (3) retina stimulator on a flexible substrate. [Reprinted with permission from Kolnsberg et al. (1999), copyright IEEE.]

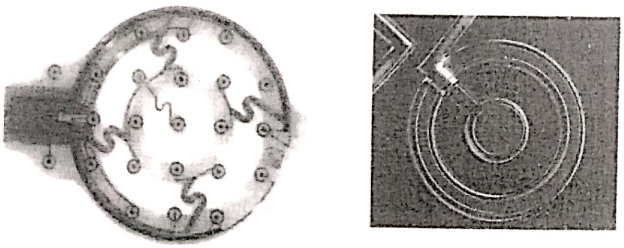

Figure 13.22 Microelectrode array on an ultra-thin PI substrate at two magnifications. [Reprinted with permission from Meyer (2002), copyright Elsevier.]

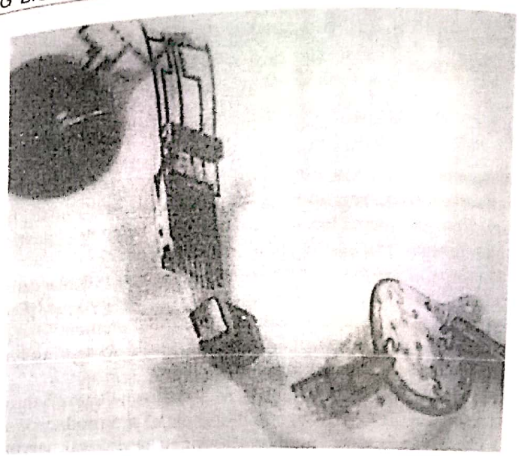

Figure 13.23 Complete assembly of the epiretinal system showing the flexibility of the translucent carrier foil and the hybrid integration of chips and surface mounted devices. [Reprinted with permission from Meyer (2002), copyright Elsevier.]

is shown in Fig. 13.23. Work is underway for placing a silicon-based microphotodiode device (MPDA) in the subretinal space, replacing the degenerated photoreceptors.

13.10 Dermabrasion

Miniaturized dermabrasion tools have been developed by Ferrara et al. (2003 and 2002). Micromachined dermabraders (*microdermabraders*) were shown to successfully abrade fine dermatological flaws in human skin, and did so better than plastic replicated devices.

The abrading microstructures were formed on silicon wafers by a bulk micromachining process based on isotropic xenon difluoride etching. Dermabraded and intact cadaver skin regions were analyzed qualitatively and quantitatively by light microscopy, image-processing techniques, and histology. The microdermabraders provided a consistently uniform cut through the epidermal layer, leaving little debris and minimal pitting. In contrast, the plastic microreplicated structures exhibited nonuniform abrading patterns and left behind more debris and eccentric pits.

13.11 Tissue Engineering

13.11.1 Introduction

Tissue is defined as an aggregation of similarly specialized cells united in the performance of a particular function and includes:

(1) *connective tissue*, a structural and binding material in the body. This includes fibroblasts, fibrinogen, collagen fibrils, and elastic fibrils. It is derived from the mesoderm and includes collagenous, elastic, mucous, reticular, osseous, and cartilaginous tissue;
(2) *reticular tissue*, a kind of connective tissue consisting of reticular cells and fibers;
(3) *interstitial tissue or stroma*, the matrix or supporting tissue of an organ, as distinguished from its parenchyma or functional element;
(4) *lymphoid tissue*, a lattice work of reticular tissue containing lymphocytes such as lymph nodes and includes the spleen;
(5) *myeloid tissue*, contained within bone marrow where erythrocytes (red blood cells) and leukocytes (white blood cells) are produced; and
(6) *nerve tissue*, which makes up the central and peripheral nervous systems and consists of neurons and other specialized cells involved in transmission of signals.

The formal science of tissue engineering emerged around 1988, and is an interdisciplinary field for the development of biological substitutes for the repair or regeneration of tissue or organ function. Tissue engineering is a potential alternative to tissue or organ transplantation.

Traditionally, tissue has been transferred from one place to another via one of three processes. *Allografting* is the process of transferring tissue from one site to another within the same host, commonly done for skin grafting after trauma or burns. *Transplantation* from another human being is commonly done for kidneys in kidney failure and bone morrow for leukemia therapy. *Xenografting* is the process of transplanting a tissue from one species of animal to another, and is commonly done for heart valves. Cadaver tissue may also be used for corneas and bone cartilage, and individuals who have suffered from a cataclysmic event and are considered brain dead may be a source of heart, kidneys, and other organs.

Microfabrication and microfluidics for tissue engineering have been recently reviewed in the literature by Andersson and van den Berg (2004). BioMEMs devices serve to advance the science of tissue engineering by providing microfluidic structures and other scaffolding systems for physical support, oxygen, and nutrition delivery, and to investigate physiologic responses. Cells need to be placed on some form of scaffolding material before tissue growth can be initiated. Viable skin, bone, cartilage, bladders, and blood vessels have been engineered, and development of muscle tissue is underway. Among the challenges to creating larger structures such as whole organs are the 3D growth required, providing oxygen and nutrition, and removing waste products.

Scaffolds are porous, often degradable structures fabricated from either natural materials (collage, fibrin) or synthetic polymers such as polyglycolide and polylactide. Complex 3D shapes are possible with micromachined pores and channels. Many cell lines, including fibroblasts, macrophages, and cancer cells survive on artifical surfaces like silicon oxide, ceramic, glass, and polymers. A well-designed scaffold allows adequate oxygenation and nutrition, and hence maintains better cell morphology, differentiation, and functionality.

Tissue engineered products may be fully functional at the time of treatment or have the potential to integrate and form the expected functional tissue upon implantation.

13.11.2 Cell patterning and bioreactors

Photolithography may be used to pattern surfaces for application of cell-adhesion material such as polylysine, fibronectin, and collagen. Matrigel is a more complex matrix that may also be used. The patterned surface is then incubated with the appropriate cell solution. Microcontact printing with a PDMS stamp and self-assembled monolayers have also been employed. Microfluidic patterning using microchannels is possible, and microfluidic devices may be used to selectively perfuse different regions of a given cell with different solutions (recall solutions may run in parallel by laminar flow through a microchannel, mixing only by diffusion) [Andersson and van den Berg, 2004]. Figure 13.24 illustrates patterning technologies.

Bioreactors are devices in which biological and/or biochemical processes develop under closely monitored and tightly controlled environmental and operating conditions [Martin et al., 2004]. Traditionally these have included industrial fermentation processing, wastewater treatment, food processing, and production of pharmaceuticals and recombinant proteins.

Seeding cells in 3D scaffolds at high densities is the basis for uniform tissue growth. The flow of a cell suspension through the pores of a scaffold may produce uniform seeding. Rotating wall vessel bioreactors (RWV) have be used to supply nutrients and remove wastes with little shear.

13.12 Cell-Based Biosensors

Park and Shuler (2003) review advances made in cell culture and microfabrication techniques. Cell-based systems have the potential for use in diagnostics, sensors, and prosthetics. Biosensors for the functional characterization and detection of drugs, pathogens, toxicants, odorants, and other chemicals have been proposed.

Cell-based biosensors are devices that contain living biological cells for monitoring physiological changes induced by exposure to different substances. They may measure physiologic, metabolic, or network processes and responses that integrate many biological components.

They are composed of two transducers, one being the cells that convert the presence of a bioactive substance into a cellular signal, the other being a sensor that converts the cellular signal into a more traditional signal detected by customary

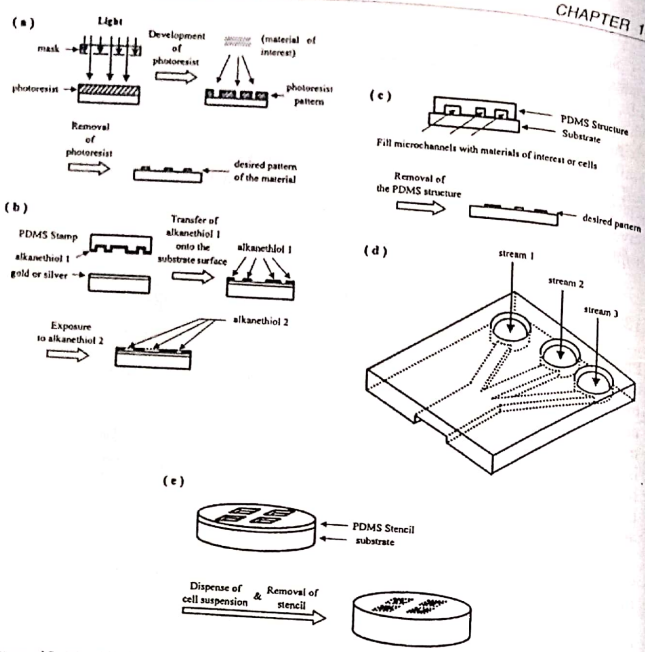

Figure 13.24 Various methods of micropatterning: (a) photolithography; (b) microcontact printing; (c) microfluidic patterning using microchannels; (d) laminar flow patterning; (e) stencil patterning. [Reprinted with permission from Park and Shuler (2003), copyright American Chemical Society.]

techniques. Microprobes may be useful in detecting cell signals in electrically excitable cells. Other techniques are employed for nonelectrically active cells.

Neuronal cells have been determined to bind specifically and sensitively with odors, drugs and toxins. Microelectrodes can measure the responses which are both substance specific and concentration dependent. Figure 13.25 shows the detection of chemical substances using neuronal networks cultured on a microelectrode array.

13.13 Homeland Security

Homeland security requirements can be classified along three lines: (1) anticipating security needs and threats; (2) deterring the efficacy of identified threats; and (3) defending against the application of these threats [Scott, 2003].

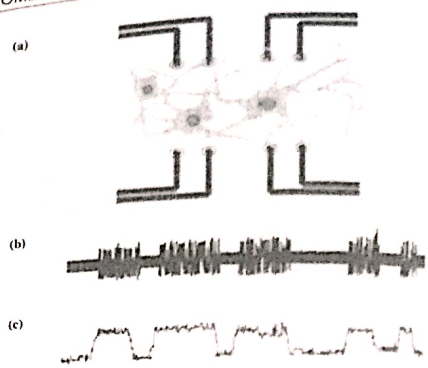

Figure 13.25 Detection of chemical substances using neuronal networks cultured on microelectrode arrays: (a) neuronal network on a microelectrode array, (b) action potential, and (c) burst, the time integral of action potential. [Reprinted with permission from Park and Shuler (2003), copyright American Chemical Society.]

The MicroHound, developed by Sandia National Laboratories, is a portable handheld "electronic nose" for sniffing out faint concentrations of explosives (Fig. 13.26). Large volumes of sampled air pass through the machine, where a metal filter captures a preconcentration of target materials. The filter is heated,

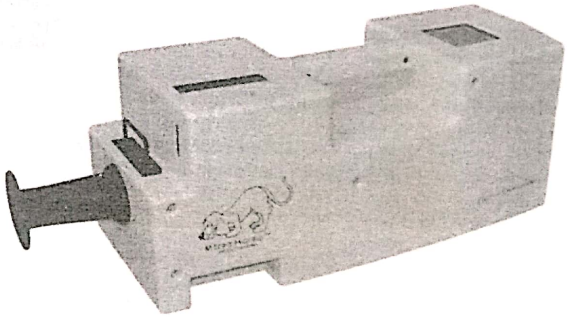

Figure 13.26 The MicroHound developed by Sandia National Laboratories for the trace detection of explosives. (Image courtesy of Sandia National Laboratories.)

re-releasing the substance in a controlled manner for detection with an ion mobility spectrometer (IMS). The 12-pound sniffer can detect explosives in parts-per-trillion concentrations, depending on the type of explosive.

Future enhancements to the MicroHound concept may include a single integrated portable platform with multiple detectors to find a variety of contraband, including radiation sources, narcotics, and hazardous chemicals.

Figure 13.27 shows the basic integration steps for a bioMEMs device for biological detection. Sandia's prototype anthrax detector under development is a hand-held device that can identify the fatty acid methyl esters (FAME) of anthrax in less than five minutes. Identification of the bacillus in minutes, rather than the hours it currently takes, is a crucial step in alerting a building's occupants to flee the deadly bacteria, as well as in activating defenses such as antianthrax foam dispersal systems.

The technique works by preconcentrating airborne particles on a tiny hotplate that acts like a skillet on a stove. The hotplate immediately vaporizes the fatty acids in anthrax's cell walls to create the FAME that form a unique fingerprint of the bacteria. A small computer program correlates the amount of mass of each ester emitted at particular times (a process called elution) with already categorized elution peaks indicative of anthrax or other diseases. Microfabrication allows the device to operate on only 150 mW of power. Sandia's chemographic and SAW analysis of gasses driven from the bacteria enables far more rapid identification of anthrax and other diseases compared to traditional methods.

Detection of aerosolized spores of *Bacillus globigii* (as surrogate species for *Bacillus anthracis*) has also been accomplished by using a biochip with

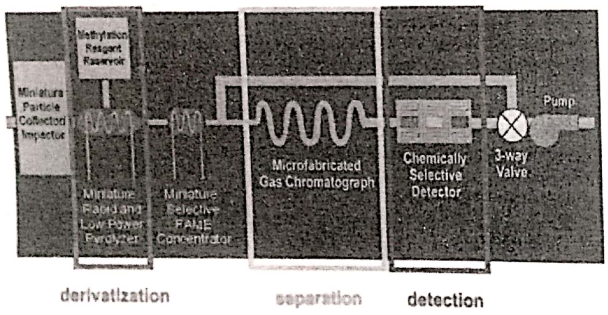

Figure 13.27 Schematic for biological detection of anthrax and other microorganisms, based on microfabricated components. Sandia has developed a prototype handheld detector that can identify the fatty methyl esters (FAME) of anthrax in less than five minutes. (Image courtesy of Sandia National Laboratories.)

antibody-based recognition and enzyme amplification [Stratis-Cullum et al., 2003].

A variety of microchip-based protocols and devices for detecting terrorist weapons has been published by Wang (2004). Microfluidic devices offer

(1) great promise for transporting the forensic laboratory to the sample source;
(2) an early warning prior to terrorist activity;
(3) rapid post-analysis of the "fingerprints" of a disaster site; and
(4) possible performance of multiple assays simultaneously.

DNA and antibody-based biochips can be used to detect deadly microprobes [Casagrande, 2002].

The University of Texas Countermeasures to Biological and Chemical Threats Program was created in 1998 and is funded by the Defense Threat Reduction Agency (DTRA) through Soldier Biological and Chemical Command (SB/CCOM) and Army Research Laboratory (ARL). The objective of the program is to eliminate or reduce the threat to the homeland posed by biological or chemical agents. Efforts include surveillance of potential biological agents, exposure, situation awareness systems, and medical responses. Current bioMEM's work includes development of high-affinity binders of threat agents and platforms upon which binders can be placed effectively. These high-affinity binders include antibodies, polynucleotides aptamers, and cDNA probes.

One interesting area being researched is *virulence factors* in pathogens. These factors are the mechanisms of pathogenicity of bacteria, including adhesion of bacteria to target tissues, and the increased transport of nutrients required for bacterial growth. Knowledge of the virulence factors may be used in the design of sensors to detect infectious agents rapidly. Various sensors under development include the "electronic tongue" for detection of antigen-antibody complexes, detection of polynucleotide complexes in gel matrices, and sensors based an antiricin aptamer [Kornguth, 2002].

The Defense Advanced Research Projects Agency (DARPA) has an active bioMEMs program. The government is motivated to do research in bioMEMs for national healthcare, biowarfare defense, and combat causality care. The DARPA Bio-Fluidic Chips (BioFlips) program considers LOC devices as useful for rapid diagnosis and treatment of combat injuries. Micro-total-analysis systems for body-fluid collection, sample preparation, self-calibration, and detection, and drug-delivery systems are envisioned [Lee, 2000].

13.14 Review Questions

1. What is minimally invasive surgery? Give examples.
2. Future point-of-care clinical diagnosis involves multifunctional integrated biochips. Outline the advantages of these systems, type of components, and integration methods.
3. A passive microvalve operates on the principle that when an abrupt change in width is effected across a microchannel fabricated on a hydrophobic